

THESIS

COUPLED STATIC FIELDS IN MAGNETO-ELECTRO-THERMOELASTIC SPHERES

Submitted by

S.L.Dinavahi Divya

Department of Civil and Environmental Engineering

In partial fulfillment of the requirements

For the Degree of Master of Science

Colorado State University

Fort Collins, Colorado

Summer 2016

Master's Committee:

Advisor: Paul R. Heyliger

Rebecca Atadero

Troy B. Holland

Copyright by S.L. Divya Dinavahi 2016

All Rights Reserved

ABSTRACT

COUPLED STATIC FIELDS IN MAGNETO-ELECTRO-THERMOELASTIC SPHERES

Smart/ intelligent materials form an integral part of adaptive and structural systems that have the capability to modify their material properties under the application of external stimuli. This study focuses on a laminated layered hollow sphere with a multi-field coupled material composed of piezo-electric and piezo-magnetic phases. When combined, these configurations create new features and properties that are absent in their constituents. The analysis of these materials requires careful consideration of the effects of interaction of the multi-field effects. In particular, the behavior of the field variables through laminate thickness is of primary interest.

In this research, a discrete-layer model is presented and applied to layered anisotropic spheres under the coupled effects of elastic, electric, magnetic, and steady-state temperature fields to study its static behavior. The model is developed in spherical coordinate system based on discrete-layer lamination theory that solves the weak form of the governing equations for the individual fields and specific boundary conditions. The through-thickness behavior of the hollow sphere was investigated by introducing Ritz-based approximations to each of the fields, which are represented layer-wise in the radial direction of the hollow sphere. The accuracy of the model is determined by comparing the results to those of exact solutions. The model is further investigated for effect of three-layer laminate scheme under various surface conditions and new results are presented for the effect of imposed thermal fields.

ACKNOWLEDGEMENTS

I would like to thank my graduate committee for all their input and advise that went into making of this thesis. In particular, I would like to extend my sincere thanks to my advisor, Dr. Paul R. Heyliger, for his support and guidance, and for his invaluable help with the Fortran code that helped in the implementation of my research.

Thanks to my friends and family for their immense support. Great thanks are also due to Leif Anderson for building this L^AT_EX document class, allowing me to meet the graduate school formatting requirements with no effort on my part.

TABLE OF CONTENTS

ABSTRACT.....	ii
ACKNOWLEDGEMENTS.....	iii
LIST OF TABLES.....	vi
LIST OF FIGURES.....	vii
Chapter 1. Introduction.....	1
1.1. Motivation.....	1
1.2. Objectives.....	3
1.3. Structure of the Report.....	4
Chapter 2. Literature Review.....	5
2.1. Piezomagnetic effect.....	5
2.2. Discrete Layer Theory.....	6
2.3. Magento-electro-thermoelastic Hollow sphere.....	8
2.4. Significance of this research.....	9
Chapter 3. Theory.....	10
3.1. Governing Equations.....	10
3.2. Constitutive Equations.....	13
3.3. The Weak Form.....	15
3.4. Discrete-Layer Approximations.....	19
Chapter 4. Numerical Examples and Results.....	22

4.1. Hollow Elastic Sphere under Uniform Pressure	23
4.2. Hollow Elastic Sphere with Thermal Load.....	24
4.3. Hollow Piezoelectric Sphere with Uniform Pressure.....	26
4.4. Layered MEE Hollow Sphere under Uniform Pressure	28
4.5. Layered MEE Hollow Sphere under Axisymmetric Loading.....	35
4.6. Hollow MEE sphere under Thermal Load	40
Chapter 5. Summary and Conclusions	45
5.1. Conclusions.....	45
5.2. Future Work.....	46
BIBLIOGRAPHY	48
APPENDIX.....	54

LIST OF TABLES

4.1	Properties for purely elastic material.....	24
4.2	Properties for MEE materials.....	44

LIST OF FIGURES

1.1	Product Property	2
3.1	Spherical coordinate system	11
3.2	Standard Mapping for Tensor Indices	14
3.3	Projections in Spherical Coordinate System	17
4.1	Geometry of layered sphere in spherical coordinates	22
4.2	Plot demonstrating the variation of radial displacement in a hollow purely elastic sphere subjected to uniform pressure	24
4.3	Variation of radial displacement and temperature change in purely elastic hollow sphere subjected to uniform temperature distribution	26
4.4	Variation of radial displacement and radial stress in hollow piezoelectric sphere subjected to uniform pressure q	28
4.5	The three physical Laminate schemes	30
4.6	Variation of radial displacements, electric and magnetic potentials, and the radial stress in layered hollow sphere composed of MEE materials subjected to uniform pressure q	34
4.7	Variation of radial magnetic displacement in layered MEE hollow sphere subjected to uniform external pressure q	35

4.8	Variation of radial displacements, electric and magnetic potentials, and the radial stress in layered hollow sphere composed of MEE materials subjected to uniform pressure q	40
4.9	Variation of radial displacement and temperature change in purely elastic hollow sphere subjected to uniform temperature distribution	43

CHAPTER 1

INTRODUCTION

1.1. MOTIVATION

In recent years, smart/intelligent materials have drawn attention from scientists and engineers for their ability to exhibit coupling between multi-physical phases. These materials creates new coupling coefficients and functions, which are completely absent in their constituents [1]. Piezoelectric material exhibits coupling between electric and mechanical fields such that it creates an electric field when deformed, and it is deformed when an electric field is applied, giving an example of two-way coupling.

In a similar fashion, a magneto-electro-thermoelastic material having piezoelectric and piezomagnetic phases exhibits coupling between mechanical, electric, and magnetic fields in the presence of a thermal environment. In addition to the piezoelectric, piezomagnetic, dielectric, electromagnetic, and magnetic permeability coefficients which are not present in its constituents, there are also pyroelectric, pyromagnetic coefficients that will not develop otherwise. The coupling occurring in this class of materials through interaction between various phases, giving rise to the so-called *product property* (Figure 1.1). These materials provide the product property strong enough to offer widespread industrial applications in various fields such as the electronics industry, nuclear industry, smart structures, biomedical devices and, superconducting devices in devices such as sensors, actuators and adaptive structures.

The magnetoelectric(ME) effect in most of the single phase multiferroic materials have been observed to be very small, which makes these materials unfit for most applications. In order to strengthen the ME effect, composites composed of piezoelectric and piezomagnetic

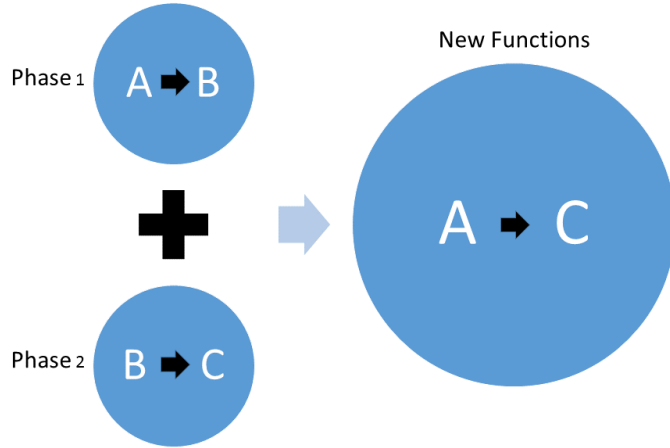


FIGURE 1.1. Product Property

phases have drawn major attention. Barium Titanate($BaTiO_3$) is an important material with piezoelectric properties because of its high dielectric constant and low dielectric loss [2]. Cobalt Ferrite($CoFe_2O_4$) is known to have the most substantial magnetostriction among the all of magnetic materials [3]. Hence, $BaTiO_3$ and $CoFe_2O_4$ make the perfect choice for piezo-electric and piezo-magnetic phase, respectively.

A smart composite material can consist of multiple layers sandwiched together, integrating piezo-electric/piezo-magnetic layers [4]. In such composites, there is a need to accurately determine the inter-laminar discontinuities due to jump in material properties at each interface. This study primarily focuses on the through-thickness behavior of the composite material, using a method that captures this behavior.

A temperature concentration in composite material causes reduction in both strength and stiffness [5],[6]. This reason makes it important to determine the temperature concentration in a composite laminate under given boundary conditions.

Discrete layer theories have been applied to numerous of geometries such as beams, cylinders, and shells. In this theory, a single coordinate is isolated and separated out from the remaining independent coordinate variables so as to allow discontinuity in the gradient of the displacement and potentials at the interfaces [7]. Across an interface, the radial normal and shear stresses are continuous, as is the radial components of electric displacement and magnetic induction. This implies that there is a break in slope as one moves across the bond line, a break that cannot be modeled with global or continuous approximation functions. By splitting this function out of the total approximation, the discontinuity can be accurately modeled. This study is based on the idea that an approximate model based on the discrete layer theory could be developed for studying the through-thickness behavior of a hollow MEE layered sphere.

1.2. OBJECTIVES

The primary objectives of this research are,

- To develop a computational model based on discrete-layer theory that combines with finite-element approximations through the hollow sphere thickness using Lagrangian interpolation polynomials in the radial direction.
- To study the through-thickness behavior of the hollow sphere made up of piezoelectric material using the proposed model.
- To determine the effect of various laminate schemes under a traction-free boundary conditions.
- To determine the response of hollow sphere under a axisymmetric loading to the varying laminate scheme.

- To study the effect of thermal field on the hollow sphere made up of a MEE material through thermoelastic coupling.

1.3. STRUCTURE OF THE REPORT

A smart material exhibits coupling between two or more different physical effects. Focusing specifically on the elastic, electric, magnetic and thermal effects, the necessary background information required to construct an approximate model where these multi-physical effects come into play will be elucidated in Chapter 1. A review of all literatures that gives us a deeper understanding of the smart materials and discrete layer models will be annotated in Chapter 3. First part of this chapter begins with overview of magnetoelectric effect and second part discusses the discrete layer models for a general laminated media, followed by review of various studies that considered magneto-electro-thermoelastic media for further understanding of the coupling effects in these materials. Discrete layer model is an approximate model that can include the coupling of physical effects and study the inter-laminar response of the composite material. Theoretical developments required towards building the discrete layer model will be presented in Chapter 3. Chapter 4 will illustrate various examples, that are solved by applying the approximate model developed. Chapter 5 will discuss the results and conclusions driven out of this study. Appendix will provide the element matrix in Ritz-based model for the coefficient matrices in the spherical coordinate system.

CHAPTER 2

LITERATURE REVIEW

This section includes a review of related studies regarding both smart materials and discrete layer models for general laminated media.

2.1. PIEZOMAGNETIC EFFECT

The magneto-electric(ME) effect is a phenomenon in which a magnetic polarization is obtained by applying a external electric field and, vice versa. The ME effect was first speculated in 1894 by Piere Curie [8] and the term *magnetolectric* was invented by Peter Debye [9]. The linear coupling of electric polarization and magnetization was formulated in the famous series of theoretical physics by Landau and Lifshitz [10] with experimentation done by Astrov [11]. Following these studies, many others observed this effect which soon enough led to the an organization named Magnetolectric Interaction Phenomenon in Crystals (MEIPIC). Theoretical and technological developments over the years led to heavy investigation on magneto-electric effect.

A multiferroic smart material which generally occurs in single phase is quite rare [12],and shows reasonably large ME effect only far below room temperature [13]. Hence many heterogeneous composites are developed where an artificial ME coupling is engineered between the order parameters of ferroelectric and ferromagnetic components, which separately do not permit the ME effect [14]. In these materials, strain is induced in the piezoelectric phase by the application of magnetic field that is mechanically coupled to induce stress in the piezoelectric phase which generates an induced voltage [15] A composite made out of piezoelectric and piezomagnetic material was first reported in 1972 by Suchtelen [16] who explained the ME

effect that results from interactions between the two phases with dissimilar properties. Multilayered composites consisting of stacked layers of piezoelectric/piezomagnetic phases found to have many applications in sensing and actuating due to their low density and superior mechanical properties [17]. The ME effect was further explored by Boomgaaed[18], particularly in $\text{BaTiO}_3\text{-CoFe}_2\text{O}_4$ composite. Various studies related to magneto-electro-elastic materials were studied using variational principles by Lee [19], He [20], and Qing et al [21].

Numerous studies have been conducted on laminated plates made up of magneto-electro-elastic(MEE) materials ([22]-[23]). A general solution procedure was constructed through analytical solutions for simply-supported and multilayered magneto-electro-elastic plates by Pan[24] and Pan and Heyliger[25]; for magneto-electro-elastic plates with polygon inclusions by Jiang et al[26]; general solutions to magneto-electro-elastic solids based on ritz-based approximations by Heyliger and Pan[27] and Heyliger et al[28].

2.2. DISCRETE LAYER THEORY

Plates and shell structures made out of laminated composite materials were often modeled as an Equivalent Single Layer (ESL) based on the Classical Laminate Theory (CLT), in which the out-of plane stress components are not considered [29]. In CLT, it is assumed that plane sections before deformation remain plane and normal to the mid plane even after deformation and normals to the middle surface have no extensions. However, this theory was applied to laminate composite structures. But it has been proved that such theories when applied to anisotropic composites suffer 30% or more errors in deflections, stresses, and frequencies [30]. In order to overcome these errors, various laminate theories were proposed based on CLT theory by Koiter (1960) [31]. For modeling 2D multilayered structures with laminates, sandwiched panels, and smart structural systems with piezoelectric layers, required revision

to Koiter's theory [32]. Adjustements such as continuity of displacements, tranverse shear, normal stresses interlaminar continuity at the interface between two adjacent layers were necessary. Significant research concerning the 3D analysis of layered plates and shells were developed confirming the significance of interlaminar continuity such as Srinivas et al, 1970 [33], Pagano and Reddy, 1994 [6], and Bhaskar et al [34].

Another refinement to CLT by taking the shear stresses into account, Reissner-Mindlin theory or the First Order Shear Deformation Theory (FSDT) achieved as an addition to laminates, which provides a global response for deflections, stresses and frequencies in rather thick composites when compared to CLT. But, both CLT and FSDT theories consider their layers as a single anisotropic layer. Both theories assume that shear stresses remain unchangeable between the layers, which make it inappropriate. However, Higher-Order Theories(HOT) presented by Reddy and Liu, 1985 [35] and Reddy,1990 [7] were able to overcome some of these defects. But again, due to dissimilar material properties at an interface, HOT also suffers from mismatch in transverse shear and normal stress at the interface. Hence, it can be concluded that ESL theories makes it impossible to accurately model the response of a laminate structure.

To obtain a accurate response at the layer level, there needs to be a model that applies the CLT, FSDT or the HOT theory to each individual layer. Garcao et al [36] modeled based on higher-order displacement theory to study the interlaminar and intralaminar effects of the laminate. Even then, research shifted towards methods with less computational effort , such as Zig-Zig theory (ZZT). In ZZT, a certain displacement or stress model is assumed in each layer and then compatibility and equilibrium conditions are used at the interface to reduce the number of unknown variables and keep them independent of the number of layers used.

This method is complicated and cumbersome since it becomes difficult to assume a continuity requirement priori for a multilayered anisotropic sphere. Preferably, a discret layer method is adopted, which allows to introduce the displacement and out-of-plane stresses continuity posteriori, by means of a through-thickness assembly of repeatable single layers. This is the approach of the present work.

Significant research was focused on the development of variational approaches to get the governing equations for these solids. There exists partial mixed theories, where the displacement fields are expressed in terms of generalized displacements and generalized surface and transverse stresses have been used on beams and plates (Rao et al (2001)[37], Rao and Desai (2004) [38]). In contrast, Hamilton's principle is a variational principle employed where no mixed theories are considered. This present work further extends such a principle to a multilayered MEE hollow sphere.

2.3. MAGENTO-ELECTRO-THERMOELASTIC HOLLOW SPHERE

In early 1974, Mindlin [39] was the first person to formulate the governing equations for a 3D linear thermo-piezoelectric medium. Later, Nowacki [40] developed general theorems and models of thermo-piezoelectricity which serves as basis of various numerical models. Altay and Dokmeci [41] constructed Euler-Lagrange equations of discontinuous thermo-piezoelectric fields. They introduced with principle of virtual work and modified it through Friedrich's transformation and equations were presented in variational form.

A smart composite made up of piezoelectric and piezomagnetic material exhibit magneto-electro-thermoelastic coupling effect which was proposed by Harshe, Nan and Benveniste ([42],[43], [44]). This assumes that such an effects does not exist in a single phase piezoelectric or piezomagnetic material. The coupling that is present between thermoelastic and electric

field in a piezoelectric material acts as a medium to sense thermomechanical disturbance from the measurement of induced electrical potential and magnetic induction.

The generic solution to an isotropic magento-electro-thermoelastic material is derived from the heat conduction equation priori, and then it is included separately to it [45]. However, it can also be included in the general model, as it is done here in this research. Smittakorn[46] studied the steady-state behavior of hygrothermopiezoelectric laminated plate for simply supported condition using three-dimensional discrete layer model. Akbarzadeh[4] developed a multi physics model to study the behavior of heterogeneous magneto-electro-elastic media under a steady state hygrothermal field. Recently, Ootao and Ishihara [47] developed the exact solution of a transient thermal stress problem of multilayered magento-electro-elastic hollow cylinder in plain strain under two conditions; unsteady and uniform surface heating. They also investigated the effect of stacking sequence, position of the interface in the stresses, electric and magnetic potential, and the effects of coupling between magnetic, electric and thermoelastic fields.

2.4. SIGNIFICANCE OF THIS RESEARCH

A discrete layer model for a hollow sphere composed of piezoelectric and piezomagnetic phases under a steady-state thermal field is formulated in static condition and to study the effects of coupling between magnetic, electric and thermoelastic fields. The through-thickness behavior of the radial and azimuthal displacement, electric and magnetic potentials and the thermal changes are measured. To best of knowledge of the author, this is the first time a computational model is developed for a multilayered MEE hollow sphere using discrete layer theory. Additionally, the effect of stacking sequence, electric and magnetic boundary conditions and an axisymmetric loading are also investigated.

CHAPTER 3

THEORY

In this chapter, the theoretical formulation for the magneto-electro-thermoelastic hollow sphere are presented. The governing equations are presented for general static response in spherical coordinates. Hamilton's principle is used to obtain the weak form for the magneto-electro-thermoelastic hollow sphere. Discrete-layer models are used to solve the equations resulting from the weak form. The layerwise theory of Reddy[7] is based on the idea that primary displacement components are represented as a linear combination of product of functions of the in-place coordinates and the functions of the thickness coordinate. This approach is used to represent the electric potential, the magnetic potential and the thermal change, in addition to the displacement components.

3.1. GOVERNING EQUATIONS

In spherical coordinates, the displacement components and the potentials are defined in the radial ($x_1 = r$), azimuthal ($x_2 = \zeta$), and circumferential ($x_3 = \theta$) directions. They are denoted as $U_1 = U_r = u(r, \zeta, \theta)$, $U_2 = U_\zeta = v(r, \zeta, \theta)$, $U_3 = U_\theta = w(r, \zeta, \theta)$, $\phi = \phi(r, \zeta, \theta)$, $\psi = \psi(r, \zeta, \theta)$ (Figure 3.1). The equations of equilibrium in the absence of body forces are:

$$\begin{aligned} \frac{\partial \sigma_{rr}}{\partial r} + \frac{1}{r \sin \zeta} \frac{\partial \sigma_{r\theta}}{\partial \theta} + \frac{1}{r} \frac{\partial \sigma_{r\zeta}}{\partial \zeta} + \frac{2\sigma_{rr} - \sigma_{\theta\theta} - \sigma_{\zeta\zeta} + \sigma_{r\zeta} \cot \zeta}{r} &= 0 \quad (3.1.1) \\ \frac{\partial \sigma_{r\zeta}}{\partial r} + \frac{1}{r \sin \zeta} \frac{\partial \sigma_{\theta\zeta}}{\partial \theta} + \frac{1}{r} \frac{\partial \sigma_{\zeta\zeta}}{\partial \zeta} + \frac{3\sigma_{r\zeta} + (\sigma_{\zeta\zeta} - \sigma_{\theta\theta}) \cot \zeta}{r} &= 0 \\ \frac{\partial \sigma_{r\theta}}{\partial r} + \frac{1}{r \sin \zeta} \frac{\partial \sigma_{\theta\theta}}{\partial \theta} + \frac{1}{r} \frac{\partial \sigma_{\theta\zeta}}{\partial \zeta} + \frac{3\sigma_{r\theta} + 2\sigma_{\theta\zeta} \cot \zeta}{r} &= 0 \end{aligned}$$

where σ_{ij} 's are the stress components in the spherical coordinates. The stress matrix is given by

$$\begin{bmatrix} \sigma_{rr} & \sigma_{r\zeta} & \sigma_{r\theta} \\ \sigma_{r\zeta} & \sigma_{\zeta\zeta} & \sigma_{\theta\zeta} \\ \sigma_{r\theta} & \sigma_{\theta\zeta} & \sigma_{\theta\theta} \end{bmatrix}$$

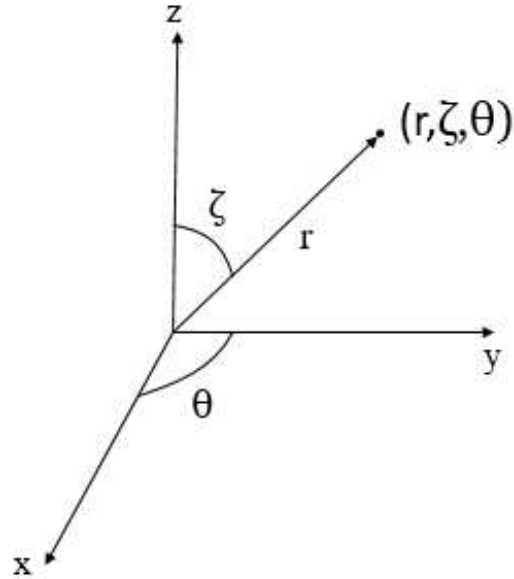


FIGURE 3.1. Spherical coordinate system

The quasi-static Maxwell equations in the absence of electric and magnetic sources are given in terms of the components of electric displacement D_r, D_θ, D_ζ and magnetic induction B_r, B_θ, B_ζ as

$$\frac{\partial D_r}{\partial r} + \frac{1}{r} \frac{\partial D_\zeta}{\partial \zeta} + \frac{2D_r}{r} + \frac{1}{r \sin \zeta} \frac{\partial D_\theta}{\partial \theta} + \frac{\cot \zeta}{r} D_\zeta = 0 \quad (3.1.2)$$

$$\frac{\partial B_r}{\partial r} + \frac{1}{r} \frac{\partial B_\zeta}{\partial \zeta} + \frac{2B_r}{r} + \frac{1}{r \sin \zeta} \frac{\partial B_\theta}{\partial \theta} + \frac{\cot \zeta}{r} B_\zeta = 0 \quad (3.1.3)$$

Additionally, the steady state head conduction equation without internal heat generation is given as

$$\frac{1}{r^2} \frac{\partial}{\partial r} \left(r^2 k_{11}^T \frac{\partial T}{\partial r} \right) + \frac{1}{r \sin \zeta} \frac{\partial}{\partial \zeta} \left(\sin \zeta k_{22}^T \frac{1}{r} \frac{\partial T}{\partial \zeta} \right) + \frac{1}{r \sin \zeta} \frac{\partial}{\partial \theta} \left(\frac{k_{33}^T}{r \sin \zeta} \frac{\partial T}{\partial \theta} \right) = 0 \quad (3.1.4)$$

The above equation of the thermal problem is from the well known Fourier's heat conduction law, which states that the heat flux is proportional to the gradient of temperature:

$$q = -k \cdot \Delta T \quad (3.1.5)$$

(or)

$$q_i = -k_{ij}^T \frac{\partial T}{\partial r_j}$$

where k^T denotes the second order thermal conductivity tensor. The negative sign indicates

that the heat flows from higher temperature to lower temperatures.

3.2. CONSTITUTIVE EQUATIONS

The constitutive equations for the class of solid considered in this study are given below. In the constitutive equations in Eq.(5), the temperature field does not fully couple with the magneto-electro-elastic field. In other words, the magneto-electro-elastic field can be affected by the temperature field through constitutive relations but the temperature field is not affected by the magneto-electro-elastic field [4] .

$$\sigma_{ij} = C_{ijkl}S_{kl} - e_{kij}E_k - q_{kij}H_k - \beta_{ij}T \quad (3.2.1)$$

$$D_i = e_{ijk}S_{ij} + \epsilon_{ij}E_j + \alpha_{ij}H_k + \gamma_i T$$

$$B_i = q_{ijk}S_{ij} + \alpha_{ij}E_j + \mu_{ij}H_k + \tau_i T$$

where S_{kl} , E_k , H_k , T are the strain tensor, electric field vector, magnetic field vector, and temperature change, respectively. C_{ijkl} , e_{kij} , q_{kij} are the fourth-order tensor of the elastic moduli, third-order tensor of piezoelectric and piezomagnetic coefficients, respectively. ϵ_{ij} , α_{ij} , μ_{ij} , β_{ij} , γ_i are second-order tensor of dielectric, electromagnetic, magnetic permeability, and thermal stress, respectively. γ_i is the the pyroelectric coefficient, and τ_i is the pyromagnetic coefficient.

Here we represent a linear theory, which implies

$$C_{ijkl} = C_{ijlk} = C_{klij} = C_{jikl}, e_{ijk} = e_{ikj}, q_{ijk} = q_{ikj}, \epsilon_{ij} = \epsilon_{ji}, \alpha_{ij} = \alpha_{ji}, \text{ and } \mu_{ij} = \mu_{ji}.$$

The notation can be contracted in standard fashion by noting that a single subscript for the stress components can represent the double subscript notation. Hence the fourth-order stiffness tensor C_{ijkl} can be written as a matrix $C_{\alpha\beta}$ which is of second order by standard mapping for tensor indices (Figure 3.2).

$$\begin{array}{rcccccc}
 ij & = & 11 & 22 & 33 & 23,32 & 13,31 & 12,21 \\
 \Downarrow & & \Downarrow & \Downarrow & \Downarrow & \Downarrow & \Downarrow & \Downarrow \\
 \alpha & = & 1 & 2 & 3 & 4 & 5 & 6
 \end{array}$$

FIGURE 3.2. Standard Mapping for Tensor Indices

In final form, the rotated elastic stiffnesses are given by $C_{11}, C_{22}, C_{33}, C_{44}, C_{55}, C_{66}, C_{12}, C_{13},$ and C_{23} . The rotated piezo-electric coefficients are $e_{11}, e_{12}, e_{13}, e_{35}, e_{26}$ and the rotated piezo-magnetic coefficients are $q_{11}, q_{12}, q_{13}, q_{35}, q_{26}$. The rotated thermal stresses are $\beta_{11}, \beta_{22}, \beta_{33}$ and the rotated hygroscopic stresses are $\xi_{11}, \xi_{22}, \xi_{33}$. The coupling coefficients which are generated from the product property, that remain non-zero due to rotation are $\epsilon_{11}, \epsilon_{22}, \epsilon_{33}, \alpha_{11}, \alpha_{22}, \alpha_{33},$ $\mu_{11}, \mu_{22}, \mu_{33}, \gamma_{11}, \gamma_{22}, \gamma_{33}, \chi_{33}, \tau_{11}, \tau_{22}, \tau_{33}$. The strain-displacement relations can be written in spherical coordinate system as

$$S_{rr} = \frac{\partial u}{\partial r} \quad (3.2.2)$$

$$S_{\zeta\zeta} = \frac{1}{r} \frac{\partial v}{\partial \zeta} + \frac{u}{r}$$

$$S_{\theta\theta} = \frac{1}{r \sin \zeta} \frac{\partial w}{\partial \theta} + \frac{\cot \zeta}{r} v + \frac{u}{r}$$

$$S_{\zeta\theta} = \frac{1}{r \sin \zeta} \frac{\partial v}{\partial \theta} + \frac{1}{r} \frac{\partial w}{\partial \zeta} - \frac{\cot \zeta}{r} w$$

$$S_{r\theta} = \frac{1}{r \sin \zeta} \frac{\partial u}{\partial \theta} + \frac{\partial w}{\partial r} - \frac{w}{r}$$

$$S_{r\zeta} = \frac{1}{r} \frac{\partial u}{\partial \zeta} + \frac{\partial v}{\partial r} - \frac{v}{r}$$

Here $S_{rr}, S_{\theta\theta}, S_{\zeta\zeta}$ are the components of the linear strain tensor, and $S_{\zeta\theta}, S_{r\theta}$, and $S_{r\zeta}$ are the components of engineering shear strain.

The electric field components E_i are related to the electrostatic potential $\phi(r, \zeta, \theta)$ using the relations

$$\begin{aligned} E_{rr} &= -\frac{\partial\phi}{\partial r} \\ E_{\zeta\zeta} &= -\frac{1}{r} \frac{\partial\phi}{\partial\zeta} \\ E_{\theta\theta} &= -\frac{1}{r \sin\zeta} \frac{\partial\phi}{\partial\theta} \end{aligned} \tag{3.2.3}$$

Similarly, the magnetic induction components B_i are related to the magnetic potential $\Psi(r, \zeta, \theta)$ using the relations

$$\begin{aligned} B_{rr} &= -\frac{\partial\Psi}{\partial r} \\ B_{\zeta\zeta} &= -\frac{1}{r} \frac{\partial\Psi}{\partial\zeta} \\ B_{\theta\theta} &= -\frac{1}{r \sin\zeta} \frac{\partial\Psi}{\partial\theta} \end{aligned} \tag{3.2.4}$$

3.3. THE WEAK FORM

A variational approach, in which either principle of virtual work or the minimum of the total potential energy of the system is used to derive the governing equations and boundary conditions, thereby to obtain the approximate solution. This is method is applicable to either linear or nonlinear theories. In this context, the principle of virtual work is used to

derive the governing equations of the layered hollow sphere. The weak form of the balance laws written in the earlier section can be written using an integral statement of virtual work for linear materials as

$$\delta \int_V H (S_{ij}, E_k, H_k, T) dV + \int_S (\bar{T}_i \delta u_i - \bar{Q} \delta \phi \bar{Q} \delta \Psi) ds = 0 \quad (3.3.1)$$

Here δ is the variational operator, which is denoted by a variation in a given quantity and, V and S are the volume and surface of the solid, \bar{T}_i , \bar{Q}_e , and \bar{Q}_m represent specified traction and surface charges, and H is the electric enthalpy per unit volume. This latter term can be expressed in terms of the strain and electromagnetic-field components as

$$\begin{aligned} H (S_{ij}, E_k, H_k, T) = & \frac{1}{2} C_{ijkl} S_{ij} S_{kl} - e_{kij} E_k S_{ij} - q_{kij} H_k S_{ij} - \alpha_{ij} E_i H_j - \frac{1}{2} \epsilon_{kl} E_k E_l - \\ & \frac{1}{2} \mu_{kl} H_k H_l - \beta_{ij} T S_{ij} + \gamma_i T E_i + \tau_i T H_i + K^T T T \end{aligned} \quad (3.3.2)$$

The weak form of the governing equations can be found out by substituting the elastic strain-displacement, the electric field-electric potential, magnetic field-magnetic potential relation and heat conduction relations and by using the δ , the variational operator on the Hamilton's principle.

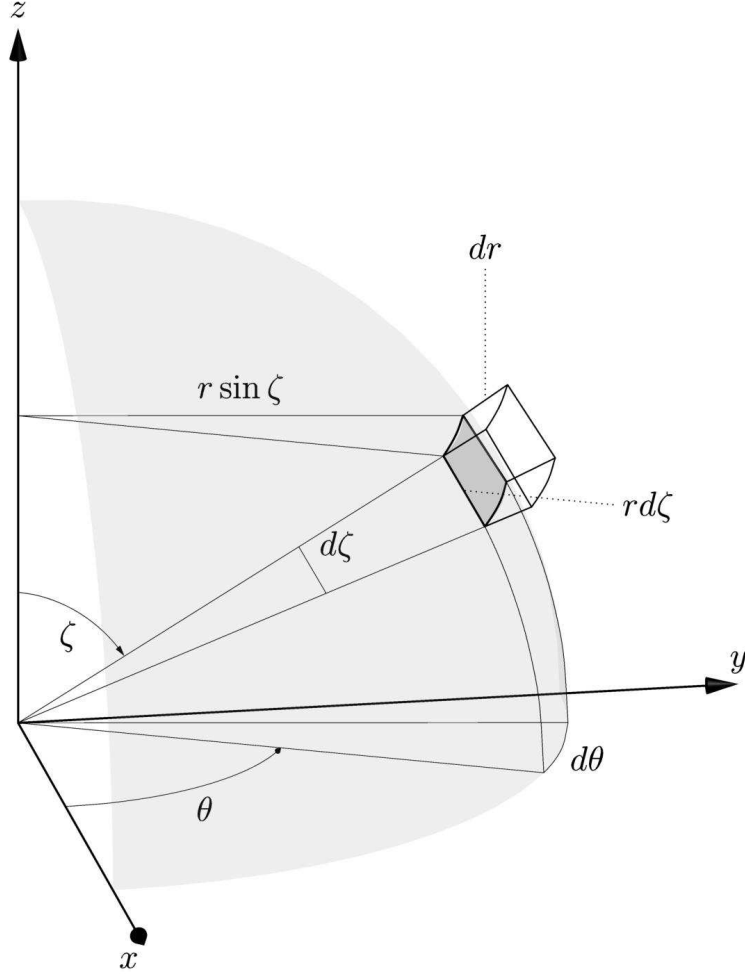


FIGURE 3.3. Projections in Spherical Coordinate System

$$0 = \int_V \left\{ C_{11} \frac{\partial u}{\partial r} \frac{\partial \delta u}{\partial r} + C_{12} \frac{\partial u}{\partial r} \left(\frac{1}{r} \frac{\partial \delta v}{\partial \zeta} + \frac{\delta u}{r} \right) + C_{13} \frac{\partial u}{\partial r} \left(\frac{1}{r \sin \zeta} \frac{\partial \delta w}{\partial \theta} + \frac{\delta u}{r} + \frac{\cot \zeta}{r} \delta v \right) + \right. \quad (3.3.3)$$

$$\begin{aligned} & C_{21} \left(\frac{1}{r} \frac{\partial v}{\partial \zeta} + \frac{u}{r} \right) \frac{\partial \delta u}{\partial r} + C_{22} \left(\frac{1}{r} \frac{\partial v}{\partial \zeta} + \frac{u}{r} \right) \left(\frac{1}{r} \frac{\partial \delta v}{\partial \zeta} + \frac{\delta u}{r} \right) + C_{23} \left(\frac{1}{r} \frac{\partial v}{\partial \zeta} + \frac{u}{r} \right) \\ & \left(\frac{1}{r \sin \zeta} \frac{\partial \delta w}{\partial \theta} + \frac{\delta u}{r} + \frac{\cot \zeta}{r} \delta v \right) + C_{33} \left(\frac{1}{r \sin \zeta} \frac{\partial w}{\partial \theta} + \frac{u}{r} + \frac{\cot \zeta}{r} v \right) \frac{\partial \delta u}{\partial r} + \\ & C_{23} \left(\frac{1}{r \sin \zeta} \frac{\partial w}{\partial \theta} + \frac{u}{r} + \frac{\cot \zeta}{r} v \right) \left(\frac{1}{r} \frac{\partial \delta v}{\partial \zeta} + \frac{\delta u}{r} \right) + \\ & C_{33} \left(\frac{1}{r \sin \zeta} \frac{\partial w}{\partial \theta} + \frac{u}{r} + \frac{\cot \zeta}{r} v \right) \left(\frac{1}{r \sin \zeta} \frac{\partial \delta w}{\partial \theta} + \frac{\delta u}{r} + \frac{\cot \zeta}{r} \delta v \right) + \end{aligned}$$

$$\begin{aligned}
& C_{44} \left(\frac{1}{r \sin \zeta} \frac{\partial v}{\partial \theta} + \frac{1}{r} \frac{\partial w}{\partial \zeta} - \frac{\cot \zeta}{r} w \right) \left(\frac{1}{r \sin \zeta} \frac{\partial \delta v}{\partial \theta} + \frac{1}{r} \frac{\partial \delta w}{\partial \zeta} - \frac{\cot \zeta}{r} \delta w \right) + \\
& C_{55} \left(\frac{1}{r \sin \zeta} \frac{\partial u}{\partial \theta} + \frac{\partial w}{\partial r} - \frac{w}{r} \right) \left(\frac{1}{r \sin \zeta} \frac{\partial \delta u}{\partial \theta} + \frac{\partial \delta w}{\partial r} - \frac{\delta w}{r} \right) + \\
& C_{66} \left(\frac{1}{r} \frac{\partial u}{\partial \zeta} + \frac{\partial v}{\partial r} - \frac{v}{r} \right) \left(\frac{1}{r} \frac{\partial \delta u}{\partial \zeta} + \frac{\partial \delta v}{\partial r} - \frac{\delta v}{r} \right) + e_{11} \frac{\partial \phi}{\partial r} \left(\frac{\partial \delta u}{\partial r} \right) + \\
& e_{12} \frac{\partial \phi}{\partial r} \left(\frac{1}{r} \frac{\partial \delta v}{\partial \zeta} + \frac{\delta u}{r} \right) + e_{13} \frac{\partial \phi}{\partial r} \left(\frac{1}{r \sin \zeta} \frac{\partial \delta w}{\partial \theta} + \frac{\delta u}{r} + \frac{\cot \zeta}{r} \delta v \right) + \\
& e_{35} \left(\frac{1}{r \sin \zeta} \frac{\partial \phi}{\partial \theta} \right) \left(\frac{1}{r \sin \zeta} \frac{\partial \delta u}{\partial \theta} + \frac{\partial \delta w}{\partial r} - \frac{\delta w}{r} \right) + e_{26} \left(\frac{1}{r} \frac{\partial \phi}{\partial \zeta} \right) \\
& \left(\frac{1}{r} \frac{\partial \delta u}{\partial \zeta} + \frac{\partial \delta v}{\partial r} - \frac{\delta v}{r} \right) + e_{11} \frac{\partial \delta \phi}{\partial r} \left(\frac{\partial u}{\partial r} \right) + e_{12} \frac{\partial \delta \phi}{\partial r} \left(\frac{1}{r} \frac{\partial v}{\partial \zeta} + \frac{u}{r} \right) + \\
& e_{13} \frac{\partial \delta \phi}{\partial r} \left(\frac{1}{r \sin \zeta} \frac{\partial w}{\partial \theta} + \frac{u}{r} + \frac{\cot \zeta}{r} v \right) + e_{35} \left(\frac{1}{r \sin \zeta} \frac{\partial \delta \phi}{\partial \theta} \right) \\
& \left(\frac{1}{r \sin \zeta} \frac{\partial u}{\partial \theta} + \frac{\partial w}{\partial r} - \frac{w}{r} \right) + e_{26} \left(\frac{1}{r} \frac{\partial \delta \phi}{\partial \zeta} \right) \left(\frac{1}{r} \frac{\partial u}{\partial \zeta} + \frac{\partial v}{\partial r} - \frac{v}{r} \right) - \\
& \epsilon_{11} \frac{\partial \delta \phi}{\partial r} \left(\frac{\partial \delta \phi}{\partial r} \right) - \epsilon_{22} \left(\frac{1}{r} \frac{\partial \phi}{\partial \zeta} \right) \left(\frac{1}{r} \frac{\partial \phi}{\partial \zeta} \right) - \epsilon_{33} \left(\frac{1}{r \sin \zeta} \frac{\partial \phi}{\partial \theta} \right) \left(\frac{1}{r \sin \zeta} \frac{\partial \phi}{\partial \theta} \right) \\
& q_{11} \frac{\partial \Psi}{\partial r} \left(\frac{\partial \delta u}{\partial r} \right) + q_{12} \frac{\partial \Psi}{\partial r} \left(\frac{1}{r} \frac{\partial \delta v}{\partial \zeta} + \frac{\delta u}{r} \right) + q_{13} \frac{\partial \Psi}{\partial r} \left(\frac{1}{r \sin \zeta} \frac{\partial \delta w}{\partial \theta} + \frac{\delta u}{r} + \frac{\cot \zeta}{r} \delta v \right) + \\
& q_{35} \left(\frac{1}{r \sin \zeta} \frac{\partial \Psi}{\partial \theta} \right) \left(\frac{1}{r \sin \zeta} \frac{\partial \delta u}{\partial \theta} + \frac{\partial \delta w}{\partial r} - \frac{\delta w}{r} \right) + q_{26} \left(\frac{1}{r} \frac{\partial \Psi}{\partial \zeta} \right) \\
& \left(\frac{1}{r} \frac{\partial \delta u}{\partial \zeta} + \frac{\partial \delta v}{\partial r} - \frac{\delta v}{r} \right) + q_{11} \frac{\partial \delta \Psi}{\partial r} \left(\frac{\partial u}{\partial r} \right) + q_{12} \frac{\partial \delta \Psi}{\partial r} \left(\frac{1}{r} \frac{\partial v}{\partial \zeta} + \frac{u}{r} \right) + \\
& q_{13} \frac{\partial \delta \Psi}{\partial r} \left(\frac{1}{r \sin \zeta} \frac{\partial w}{\partial \theta} + \frac{u}{r} + \frac{\cot \zeta}{r} v \right) + q_{35} \left(\frac{1}{r \sin \zeta} \frac{\partial \delta \Psi}{\partial \theta} \right) \\
& \left(\frac{1}{r \sin \zeta} \frac{\partial u}{\partial \theta} + \frac{\partial w}{\partial r} - \frac{w}{r} \right) + q_{26} \left(\frac{1}{r} \frac{\partial \delta \Psi}{\partial \zeta} \right) \left(\frac{1}{r} \frac{\partial u}{\partial \zeta} + \frac{\partial v}{\partial r} - \frac{v}{r} \right) - \\
& \mu_{11} \frac{\partial \delta \Psi}{\partial r} \left(\frac{\partial \delta \Psi}{\partial r} \right) - \mu_{22} \left(\frac{1}{r} \frac{\partial \Psi}{\partial \zeta} \right) \left(\frac{1}{r} \frac{\partial \Psi}{\partial \zeta} \right) - \mu_{33} \left(\frac{1}{r \sin \zeta} \frac{\partial \Psi}{\partial \theta} \right) \left(\frac{1}{r \sin \zeta} \frac{\partial \Psi}{\partial \theta} \right) + \\
& \alpha_{11} \frac{\partial \phi}{\partial r} \frac{\partial \delta \Psi}{\partial r} + \alpha_{22} \left(\frac{1}{r} \frac{\partial \phi}{\partial \zeta} \right) \left(\frac{1}{r} \frac{\partial \Psi}{\partial \zeta} \right) + \alpha_{33} \left(\frac{1}{r \sin \zeta} \frac{\partial \phi}{\partial \theta} \right) \left(\frac{1}{r \sin \zeta} \frac{\partial \Psi}{\partial \theta} \right) +
\end{aligned}$$

$$\begin{aligned}
& \alpha_{11} \frac{\partial \Psi}{\partial r} \frac{\partial \delta \phi}{\partial r} + \alpha_{22} \left(\frac{1}{r} \frac{\partial \Psi}{\partial \zeta} \right) \left(\frac{1}{r} \frac{\partial \phi}{\partial \zeta} \right) + \alpha_{33} \left(\frac{1}{r \sin \zeta} \frac{\partial \Psi}{\partial \theta} \right) \left(\frac{1}{r \sin \zeta} \frac{\partial \phi}{\partial \theta} \right) - \\
& \beta_{11} \frac{\partial \delta u}{\partial r} T + \beta_{22} \frac{\delta u}{\partial r} T + \beta_{33} \frac{\delta u}{\partial r} T - \gamma_1 \frac{\partial \delta \phi}{\partial r} T + \tau_1 \frac{\partial \delta \Psi}{\partial r} T + \\
& \frac{k_1^T}{r^4} \left(r^2 \frac{\partial T}{\partial r} + 2rT \right) \left(r^2 \frac{\partial \delta T}{\partial r} + 2r\delta T \right) + \\
& -\rho \dot{u} \delta \dot{u} - \rho \dot{v} \delta \dot{v} - \rho \dot{w} \delta \dot{w} \} \quad r^2 \sin \zeta dr d\theta d\zeta
\end{aligned}$$

3.4. DISCRETE-LAYER APPROXIMATIONS

The approximations are set according the general laminate theory of Reddy[35] for an elastic laminate for displacements. This theory is further extended to include the electric potential , the magnetic potential, and the temperature change. The approximations for the displacement components and the potential variables, using finite linear combinations are of the form

$$\begin{aligned}
u(r, \zeta, \theta) &= \sum_{j=1}^n u_j N_j^{u_r}(r) N^{u_s}(\zeta, \theta) & \delta u &= N_i^{u_r}(r) N^{u_s}(\zeta, \theta) \\
v(r, \zeta, \theta) &= \sum_{j=1}^n v_j N_j^{v_r}(r) N^{v_s}(\zeta, \theta) & \delta v &= N_i^{v_r}(r) N^{v_s}(\zeta, \theta) \\
w(r, \zeta, \theta) &= \sum_{j=1}^n w_j N_j^{w_r}(r) N^{w_s}(\zeta, \theta) & \delta w &= N_i^{w_r}(r) N^{w_s}(\zeta, \theta) \\
\phi(r, \zeta, \theta) &= \sum_{j=1}^n \phi_j N_j^{\phi_r}(r) N^{\phi_s}(\zeta, \theta) & \delta \phi &= N_i^{\phi_r}(r) N^{\phi_s}(\zeta, \theta) \\
\psi(r, \zeta, \theta) &= \sum_{j=1}^n \psi_j N_j^{\psi_r}(r) N^{\psi_s}(\zeta, \theta) & \delta \psi &= N_i^{\psi_r}(r) N^{\psi_s}(\zeta, \theta)
\end{aligned} \tag{3.4.1}$$

$$T(r, \zeta, \theta) = \sum_{j=1}^n T_j N_j^{T_r}(r) N^{T_s}(\zeta, \theta) \quad \delta T = N_i^{T_r}(r) N^{T_s}(\zeta, \theta)$$

where $u, v,$ and w are the displacement components in the r, ζ and θ coordinate directions respectively in the, ϕ is the electric potential, ψ is the magnetic potential and T is the temperature change. $u_j, v_j, w_j, \phi_j, \psi_j$ are constants, and the N 's are the approximation or basis functions.

In the above expressions, it can be seen that the one dimensional Lagrangian Interpolation polynomial $N_j^{ur}(r)$ is used to represent the through-thickness approximation for displacement in the radial direction, same representation is used for other variables as well. And approximations for the spherical surface is given by two-dimensional functions in (ζ, θ) . There are a total of n layers and $(n+1)$ interfaces through the thickness. Finally, the governing equations can be expressed in a matrix form by replacing the variables with the corresponding approximating functions, as shown in Eq.(3.4.2).

The explicit nature of $[K]$ is a function of the approximation functions used. Depending on these functions, a combination of analytic and numerical integration techniques are used to evaluate the individual elements of these matrices. Numerical integration is particularly useful when the elastic stiffnesses vary as a function of position and the resulting integrals are difficult to evaluate in closed form. For the problem considered in this thesis, purely analytical intergration was sufficient. The explicit forms of the coefficient matrices for the spherical coordinate systems are given in Appendix.

$$\begin{bmatrix}
[K^{11}] & [K^{12}] & [K^{13}] & [K^{14}] & [K^{15}] & [K^{16}] \\
[K^{21}] & [K^{22}] & [K^{23}] & [K^{24}] & [K^{25}] & [K^{26}] \\
[K^{31}] & [K^{32}] & [K^{33}] & [K^{34}] & [K^{35}] & [K^{36}] \\
[K^{41}] & [K^{42}] & [K^{43}] & [K^{44}] & [K^{45}] & [K^{46}] \\
[K^{51}] & [K^{52}] & [K^{53}] & [K^{54}] & [K^{55}] & [K^{56}] \\
[0] & [0] & [0] & [0] & [0] & [K^{66}]
\end{bmatrix}
\begin{Bmatrix}
\{u\} \\
\{v\} \\
\{w\} \\
\{\phi\} \\
\{\psi\} \\
\{T\}
\end{Bmatrix}
=
\begin{Bmatrix}
\{F^1\} \\
\{F^2\} \\
\{F^3\} \\
\{F^4\} \\
\{F^5\} \\
\{F^6\}
\end{Bmatrix}
\quad (3.4.2)$$

CHAPTER 4

NUMERICAL EXAMPLES AND RESULTS

Several example problems are considered to demonstrate the accuracy of the computational model developed in this study under varying boundary conditions. The examples initially use purely elastic and piezoelectric hollow sphere, with later examples including magneto-electro-elastic(MEE) layers. A thermal field is applied to hollow sphere composed of MEE layers. A hollow MEE sphere consisting of n layers and $n-1$ interfaces that is considered in this study is shown in Figure 4.1, based on which all the problems below are solved.

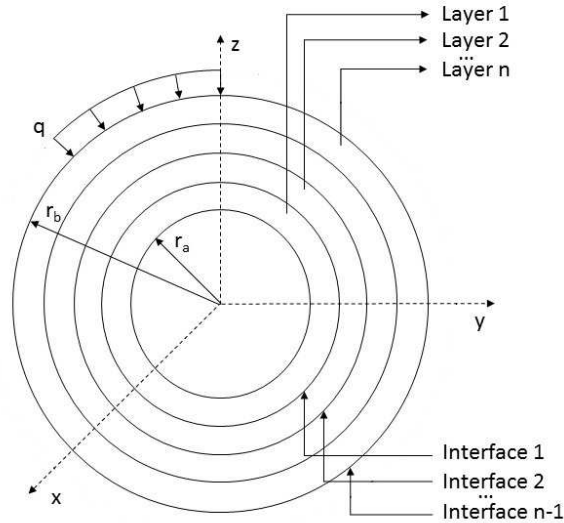


FIGURE 4.1. A hollow MEE sphere made of n layers and $n-1$ interfaces, with its inner radius at r_a and outer radius r_b subjected to surface loading q . Both surfaces are subjected to induced traction boundary conditions

4.1. HOLLOW ELASTIC SPHERE UNDER UNIFORM PRESSURE

In this section, the analytical solution for pressurized purely elastic hollow sphere is examined to verify the discrete-layer model with the exact solution. This example is chosen because there is an exact solution for the displacement of pressurized hollow sphere(Section 4.1.4)[48]. By comparison, the present model can be validated.

A homogeneous hollow sphere is assumed to be made up of a purely elastic material with no body forces acting on it. The inner radius of the sphere, r_a is half of the outer radius r_b and a uniform external pressure q is applied on the outer surface of the sphere.

A fortran code is written to find out the displacement field in the radial direction according to the discrete layer theory for a purely elastic hollow sphere. Material coefficients used for this problem are listed in Table 4.1. The radial displacement in its dimensionless form is given by $u_r C_{44}/r_b q$. Here, u_r is the only non-zero variable.

It was evident that the results obtained matched explicitly with the exact solution with a fairly small number of layers (10 layers), having accuracy to within 5 decimal places.

Figure 4.2 shows the results obtained from analytical and theoretical solution of displacement field in the radial direction. By solving this problem, the accuracy of the our model was checked and it served as a basis for solving other problems with many other variables and complicated boundary conditions.

TABLE 4.1. Properties for purely elastic material. The units of C_{ij} 's are N/m^2

Property	Purely Elastic Material
C_{11}	3.5
C_{12}	1.5
C_{13}	1.5
C_{22}	3.5
C_{23}	1.5
C_{33}	3.5
C_{44}	1.0

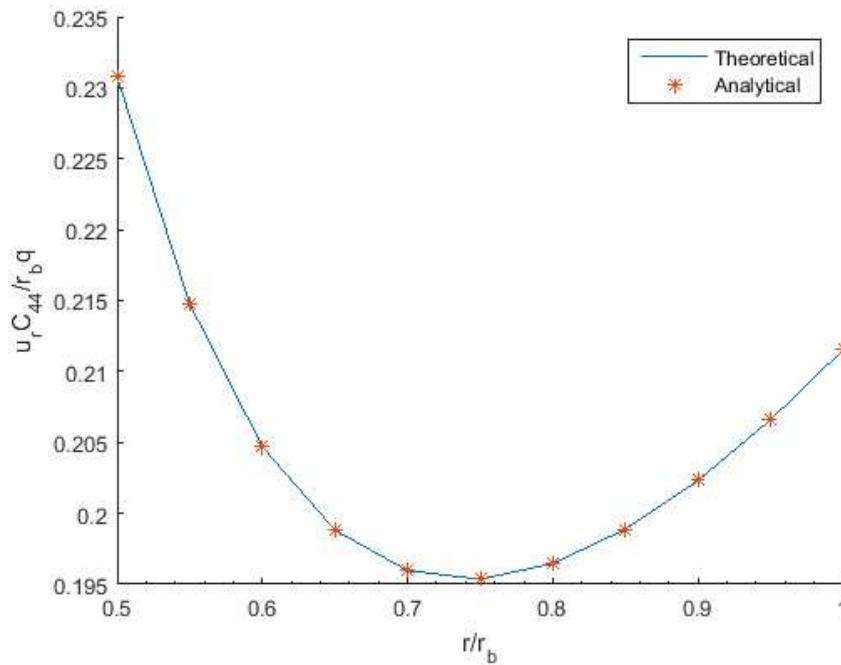


FIGURE 4.2. Plot demonstrating the variation of radial displacement $u_r C_{44} / (r_b q)$ along the radial direction (r/r_b) in a hollow sphere made up of purely elastic material applied with an uniform external pressure of σ_0 / C_{max} on its outer surface r_b

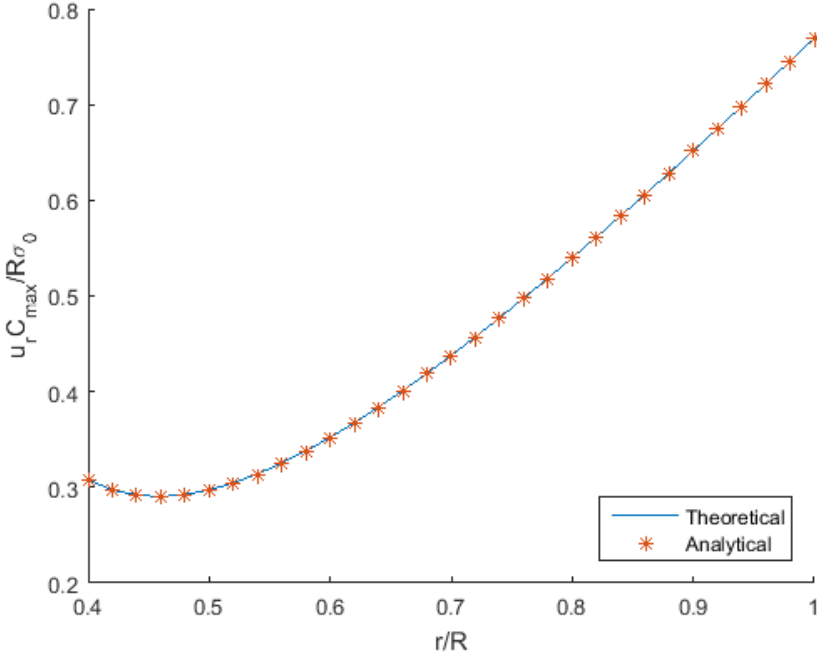
4.2. HOLLOW ELASTIC SPHERE WITH THERMAL LOAD

Similar to the previous problem, this section aims to check the accuracy of the model under a steady state thermal load. There is an exact solution for the displacement and thermal change in a hollow sphere (Section 4.1.6)[48]. A uniform temperature distribution is applied to the outer and inner surfaces of the homogeneous hollow elastic sphere. The

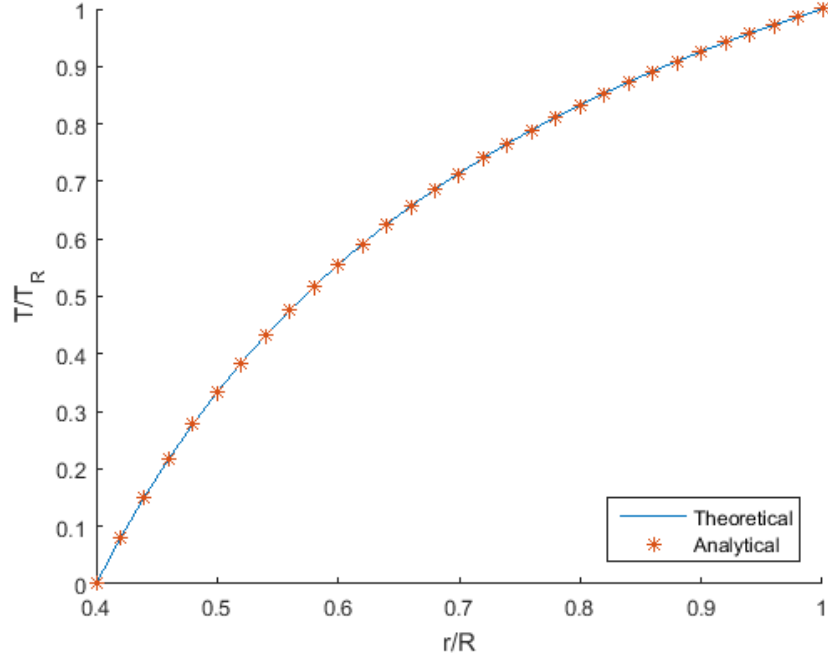
boundary condition is imposed as

$$T(0.4R, \zeta, \theta) = 0 \quad T(R, \zeta, \theta) = 1.0 \tag{4.2.1}$$

The material properties used for this problem are listed in Table 4.1. The only non-zero variables for this problem are u_r and T . The dimensionless radial displacement and temperature change obtained by discrete layer (analytical) model is presented in comparison to the exact solutions in Figures 4.3a and 4.3b, respectively. The results obtained were a perfect match to that of the exact solution by using 30 number of layers upto 5 decimal places.



(a) Variation of radial displacement in purely elastic hollow sphere



(b) Variation of temperature in purely elastic hollow sphere

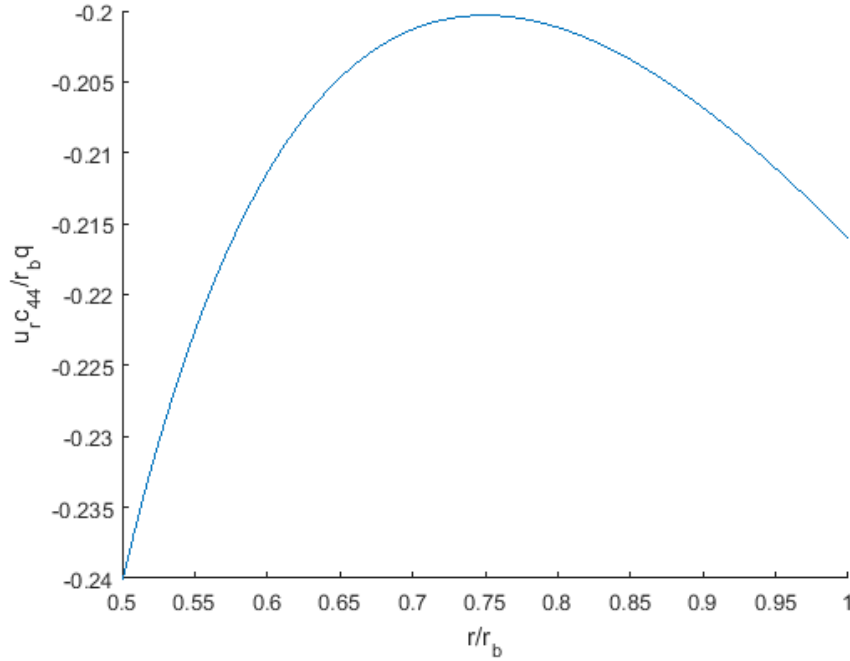
FIGURE 4.3. Plot demonstrating the variation of (a) dimensionless radial displacement $u_r C_{44}/(qr_b)$ and (b) dimensionless temperature change (T/T_R) along the radial direction (r/R) in a purely elastic hollow sphere applied with an uniform temperature distribution along its radial direction.

4.3. HOLLOW PIEZOELECTRIC SPHERE WITH UNIFORM PRESSURE

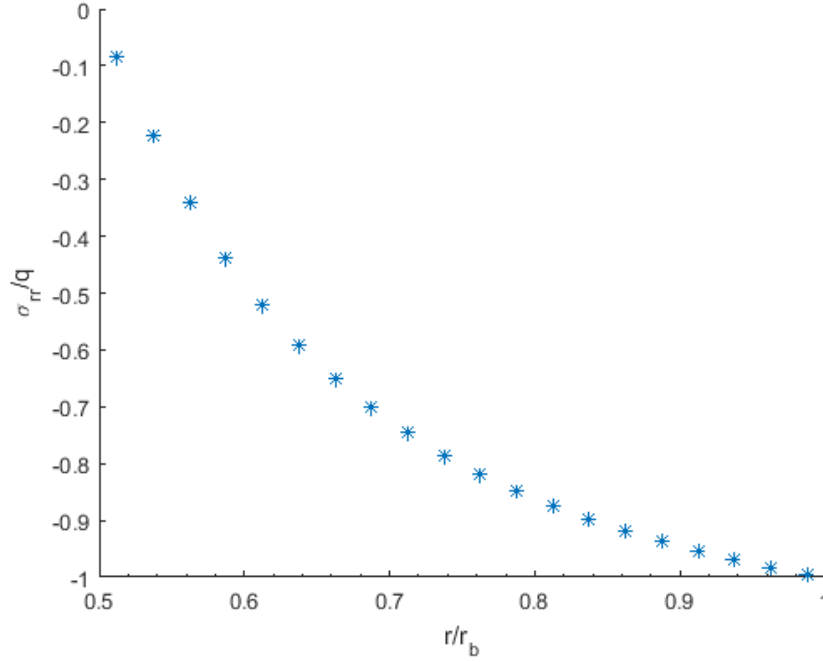
As a special case of the general formulation, the case of a piezoelectric hollow sphere is considered. This problem has been treated by Chen et al [23],[49]. This problem was chosen as an idea to replicate the results by Chen and to study how our model behaves under an electric boundary condition. For this problem, a hollow sphere composed of piezoelectric material is considered. The sphere is hollow with its inner radius r_a exactly half of the outer radius r_b . The magnetic and thermal fields are exactly zero. On the inner face of the sphere, the electric displacement $D_r = 0$ and the face is also traction-free and hence $\sigma_{rr} = 0$. On the outer face, $D_r = 0$ $\sigma_{rr} = -q$. Hence, u_r and ϕ remain non-zero variables for this problem. Chen and co-workers [49] use the material properties of Dunn and Taya [51], but their paper

contains a typo for the piezoelectric coefficients of BaTiO₃. The corrected values are given in Table 4.2.

The approximations for radial displacement u_r and electric potential ϕ are taken to be constant in the (ζ, θ) directions ie., $N_i(\zeta, \theta) = 1$. Only the radial variation $N_j(r)$ is captured by the discrete-layer approximation. A total of 30 layers was used to represent the thickness variation of these two variables. The resulting distributions of dimensionless radial displacement and radial stress are shown in Figure 4.4a and Figure 4.4b, respectively. These results are virtually identical to the solutions obtained by analytical methods [49, 23].



(a) Variation of radial displacement in hollow piezoelectric sphere subjected to uniform pressure q



(b) Variation of radial stress in hollow piezoelectric sphere subjected to uniform pressure q

FIGURE 4.4. Plot demonstrating the variation of (A) dimensionless radial displacement $u_r C_{44}/(q r_b)$ and (B) dimensionless radial stress $\sigma_{rr}/q C_{44}$ along the radial direction (r/r_b) in a hollow piezoelectric sphere composed of BaTiO_3 applied with an uniform external pressure q on its outer surface r_b

4.4. LAYERED MEE HOLLOW SPHERE UNDER UNIFORM PRESSURE

The problem of the coupled magneto-electro-elastic layered sphere has recently been considered by Chen and co-workers [23]. One of their examples has also been studied by a different model by Chen [49]. Each of these provides a good means of comparison for three of the fields considered in this study (elastic, electric, and magnetic fields). The spherically symmetric case of a sphere composed of dissimilar piezoelectric, magnetostrictive, or magnetoelectroelastic spheres are considered. For these analyses, there are three material types: BaTiO_3 (denoted subsequently by B), CoFe_2O_4 (denoted subsequently by F), and a material designated as MEE that is assumed to be composed of 50 percent BaTiO_3 and 50 percent CoFe_2O_4 [50]. All properties for these materials are given in Table 4.2.

A uniform pressure on the outer surface of the sphere is specified as $\sigma_{rr} = -\sigma_0 = -q$. The inner surface of the sphere is traction free. On both inner and outer surfaces, the electrostatic potential and magnetic potentials are both specified to be zero.

The hollow sphere has an outer radius of R and an inner radius of $0.4R$. When layered, constant thicknesses of $0.2R$ are assumed for each layer of the material. Three different physical lamination schemes are considered: 1) a 3-layer system of B/F/B, 2) a 3-layer system of F/B/F, and 3) a single homogeneous layer of MEE material. The three laminate schemes are presented in the Figure 4.5.

Once again, the (ζ, θ) dependence of the radial displacement and the two potentials can be approximated with a single term since there is no variation in pressure over the exterior surface and $N_i(\zeta, \theta) = 1$ for all the variables. For this problem u_r , ϕ and ψ are the non-zero variables. Hence for n layers there are a total of $3*(n+1)$ equations and unknowns that need to be solved. The dimensionless results are shown in Figures 4.6a to 4.6f. The two vertical dashed line represent the interfaces of the layered MEE sphere. There is excellent agreement with the results of chen [23]. It can be clearly seen from Figure 4.6a, 4.6b and 4.6c that the radial displacement, electrostatic and magnetic potential have an effect due dissimilar layers of B/F/B and F/B/F through the laminate thickness. Whereas, these results did not see a drastic change in its slope through the thickness of the homogeneous MEE laminate scheme.

It is important to note that the boundary conditions that were set at zero electrostatic field and magnetic fields for this problem has been satisfied, which again proves our model to be legitimate.

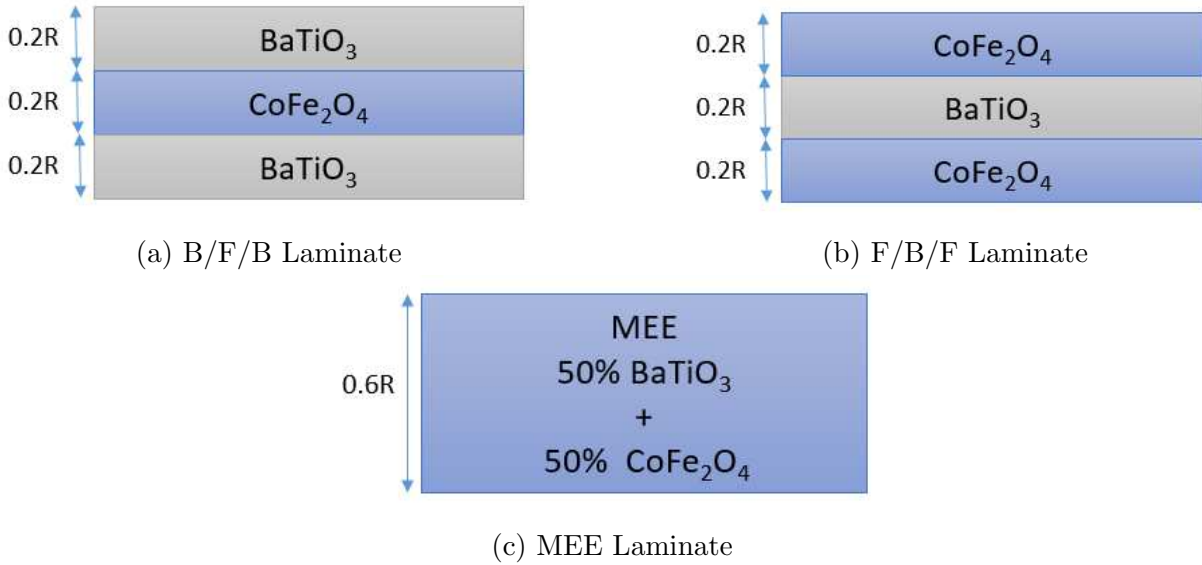
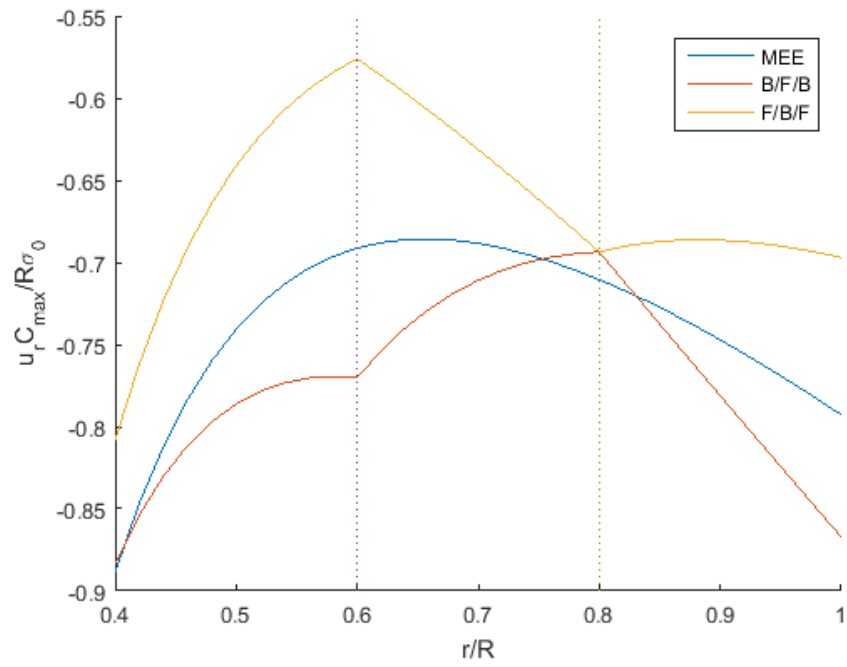
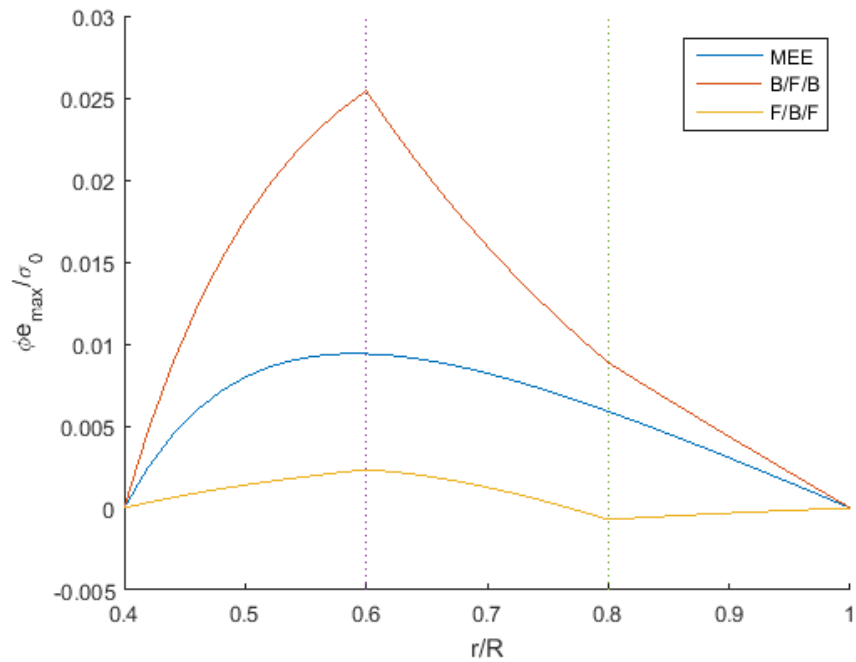


FIGURE 4.5. Each of the three types of laminate schemes above consists of combinations of piezoelectric barium titanate BaTiO₃ and magnetostrictive cobalt ferrite CoFe₂O₄, integrated together to form a smart composite.

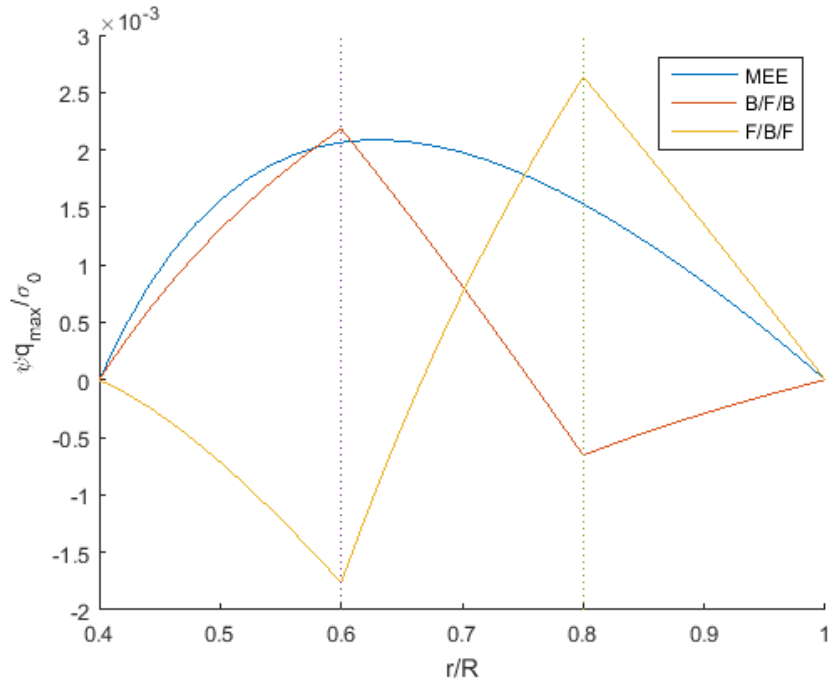
Further from Figure 4.6d, it is evident that the radial stresses have been impacted the least at the interfaces of the layered schemes when compared to the homogeneous MEE laminate. From Figure 4.6e and 4.6f, it is observed that MEE laminate has the most significant values for electric displacement and magnetic induction when compared to the other layered laminates.



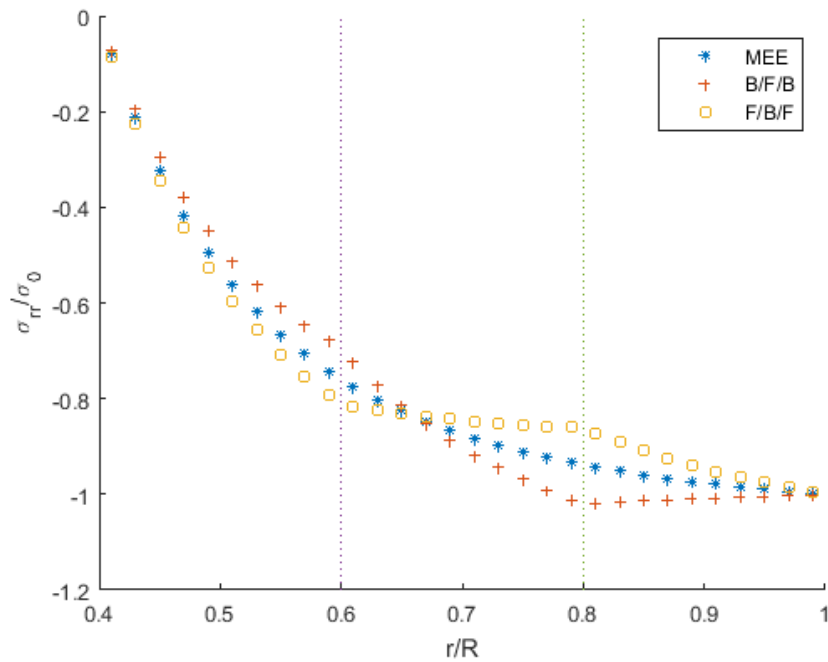
(a) Variation of radial displacement component in layered hollow sphere composed of MEE materials subjected to uniform external pressure q



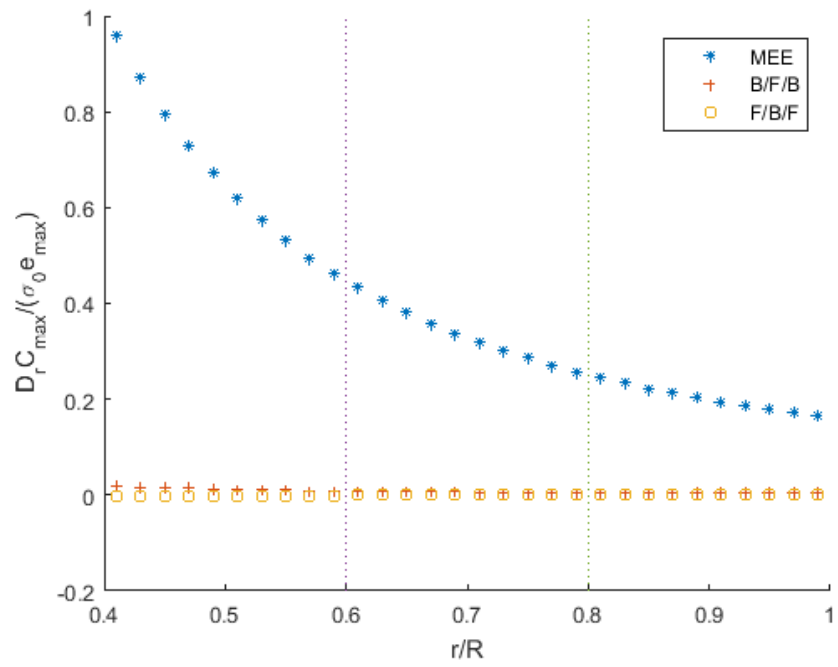
(b) Variation of electric potential component in layered hollow sphere composed of MEE materials subjected to uniform external pressure q



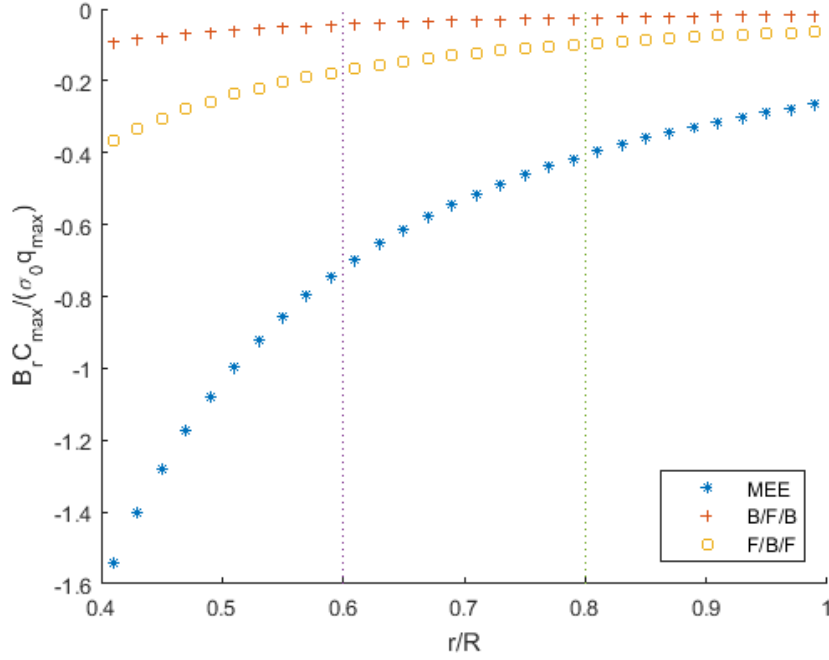
(c) Variation of magnetic potential component in layered hollow sphere composed of MEE materials subjected to uniform external pressure q



(d) Variation of radial stress component in layered hollow sphere composed of MEE materials subjected to uniform external pressure q



(e) Variation of radial electric displacement in layered hollow sphere composed of MEE materials subjected to uniform external pressure q



(f) Variation of radial magnetic displacement in layered hollow sphere composed of MEE materials subjected to uniform external pressure q

FIGURE 4.6. Plot demonstrating the variation of (A) dimensionless radial displacement $u_r C_{44}/(qr_2)$, (B) dimensionless electric potential $\phi e_{max}/\sigma_0$, and (C) dimensionless magnetic potential component $\psi q_{max}/\sigma_0$ (D) dimensionless radial stress σ_{rr}/σ_0 , (E) dimensionless radial electric displacement $D_r C_{max}/\sigma_0 e_{max}$, and (F) dimensionless radial magnetic displacement $B_r C_{max}/\sigma_0 q_{max}$ along the radial direction (r/R) in hollow sphere composed of magneto-electro-elastic (MEE) materials applied with an uniform external pressure of q on its outer surface r_b .

4.5. LAYERED MEE HOLLOW SPHERE UNDER AXISYMMETRIC LOADING

For this problem, the layered MEE hollow spheres (Figure 4.5) are considered from the previous section. But a more complex loading of axisymmetric external loading (Figure 4.7) on outer radius r_b is applied, which is of the form:

$$\sigma_{rr}(R, \zeta, \theta) = \sigma_o P_2^0(\cos\zeta) = \sigma_o \frac{1}{2}(3 \cos^2 \zeta - 1) \quad (4.5.1)$$

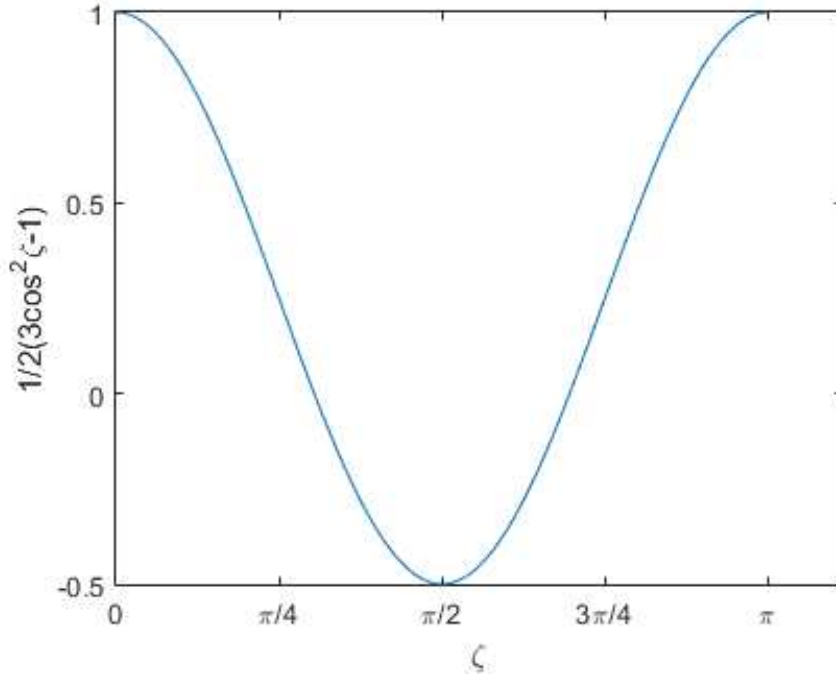


FIGURE 4.7. Variation of radial magnetic displacement in layered MEE hollow sphere subjected to uniform external pressure q .

This example can serve to show the sequential ordering of approximation functions as loadings become more complex. In this case, there is no θ dependence on the loading, and hence all fields should also depend only on the radial and azimuthal coordinates. Lower order terms in ζ can be included in the approximations for u_r , u_ζ , ϕ , and ψ . These are built

as follows:

$$N_1^{u_s}(\zeta) = N_1^{v_s}(\zeta) = N_1^{\phi_s}(\zeta) = N_1^{\Psi_s}(\zeta) = 1 \quad (4.5.2)$$

$$N_2^{u_s}(\zeta) = N_2^{\phi_s}(\zeta) = N_2^{\Psi_s}(\zeta) = \cos \zeta$$

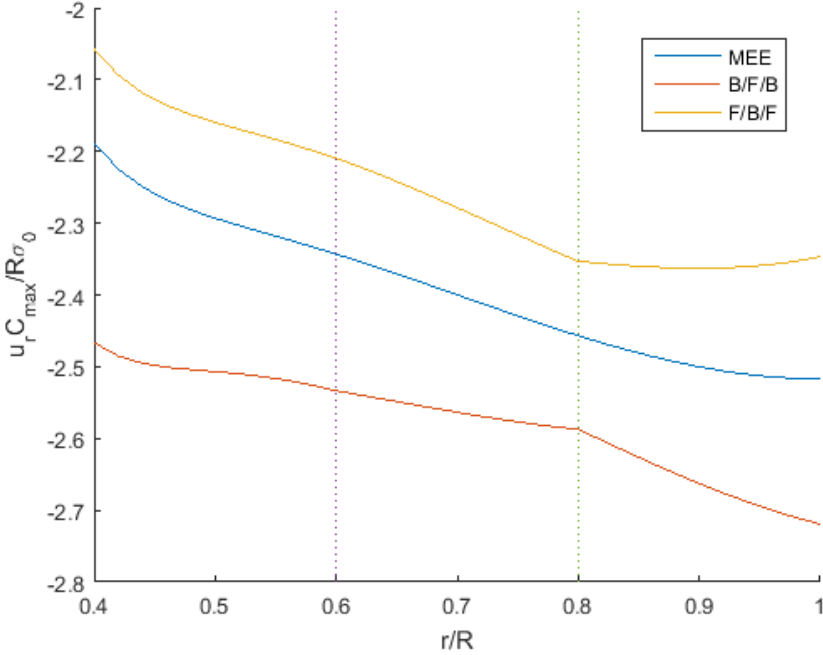
$$N_2^{v_s}(\zeta) = \sin \zeta$$

$$N_2^{u_s}(\zeta) = N_2^{\phi_s}(\zeta) = N_2^{\Psi_s}(\zeta) = (3 \cos^2 \zeta - 1)$$

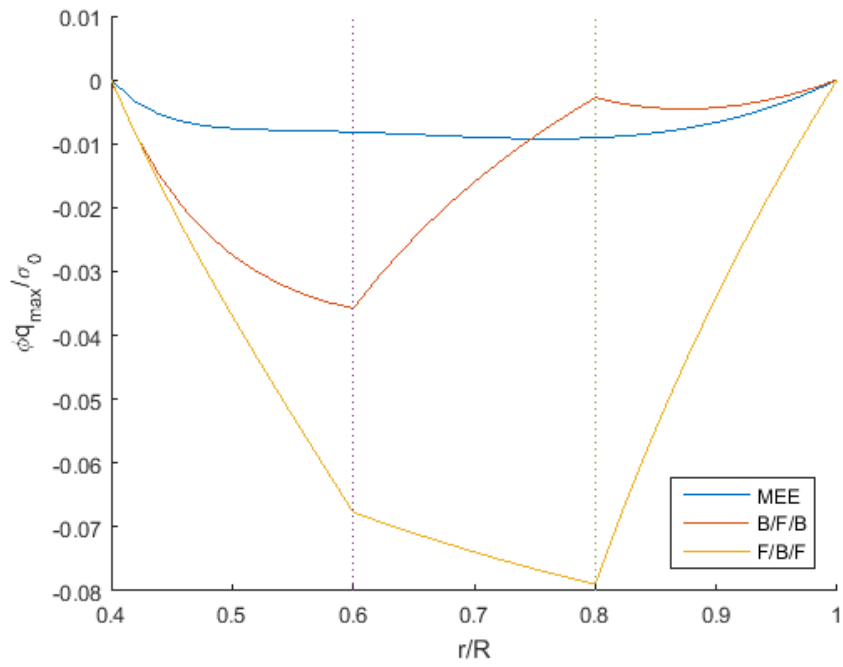
Structuring the approximations in this order is formulated so that approximations are built sequentially and helps to ensure that low-order response in terms of spatial complexity is captured. For this family of approximations, there are 3 approximations for the 3 of the variables and 2 approximations for the azimuthal displacement. Hence in general, for n layers, there are a total of $(3)(3)(n+1) + (2)(1)(n+1)$ or $11(n+1)$ equations and unknowns. However, the nature of the loading and approximations is such that the submatrices that connect the various approximations are all zero except for those with the third approximation for u_r , ϕ , and Ψ and the second approximation for u_ζ .

The dimensionless results are shown in Figures 4.8a -4.8f. In this case, from Figure 4.8a, it can be noted that radial displacement is not affected by layering of the laminate. However, from Figure 4.8b and 4.8c, it can be observed that the electrostatic potential and magnetic potential have significant effects due to the layered laminate schemes of B/F/B and F/B/F when compared to homogeneous MEE laminate. It is interesting to note that this case to have seen different behavior for electric displacement and magnetic induction from previous section with uniform pressure loading. Here, the laminate sequence B/F/B

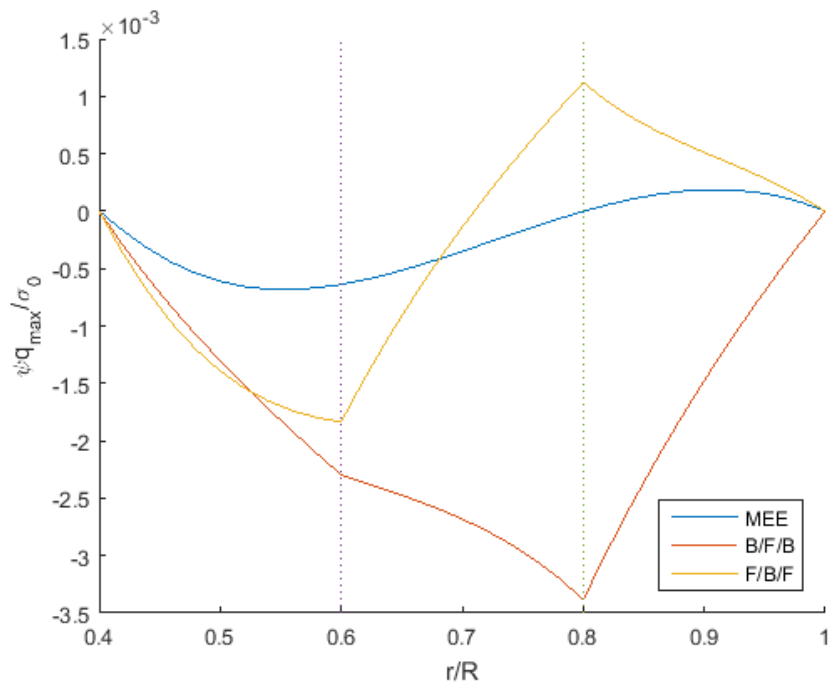
showed the most significant electric displacement and F/B/F laminate exhibited highest magnitude of magnetic induction, which was true for both the cases on the innermost layer. Once again, the radial stress did not show any visible change in its behavior with 3-layered laminate schemes when compared to the homogeneous MEE layer.



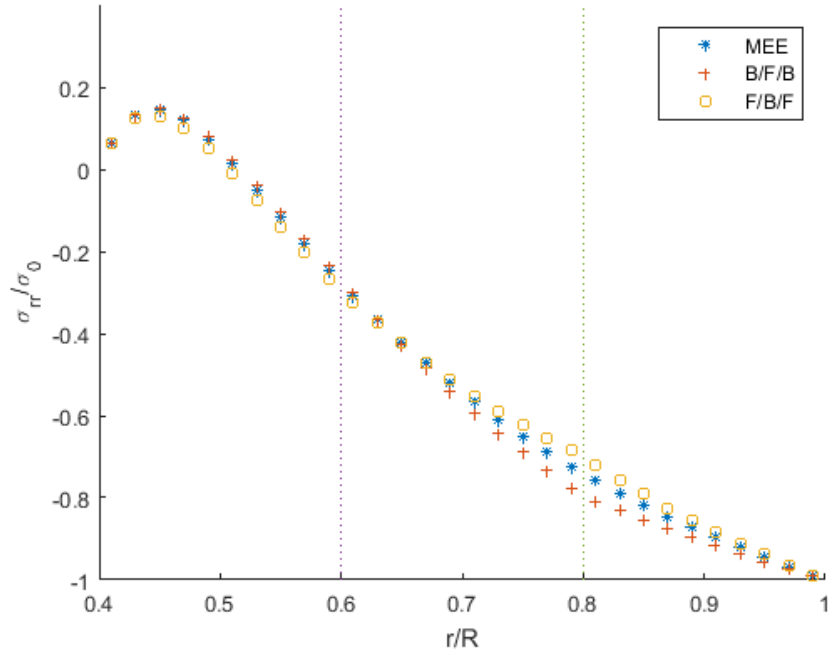
(a) Variation of radial displacement component in layered hollow sphere composed of MEE materials subjected to uniform external pressure q



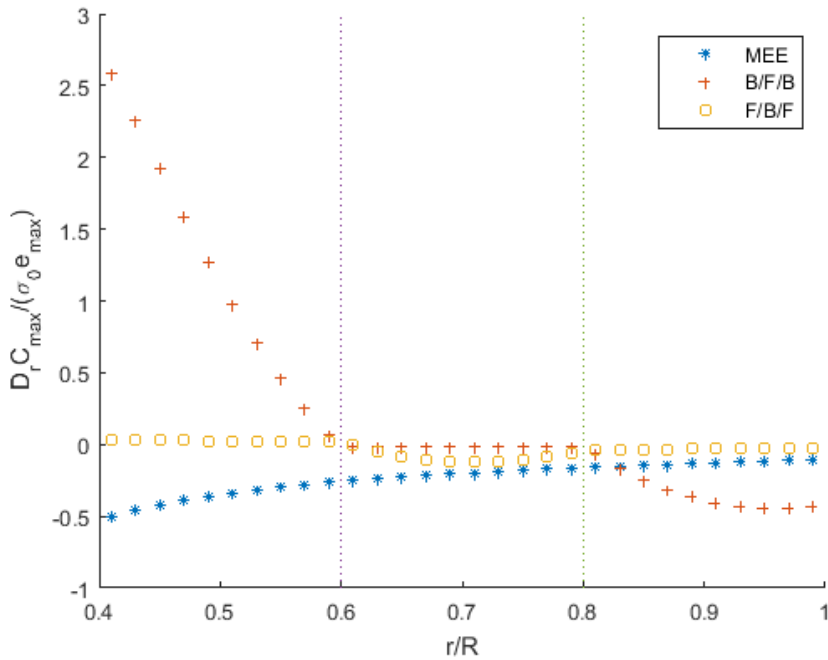
(b) Variation of electric potential component in layered hollow sphere composed of MEE materials subjected to axisymmetric external pressure q



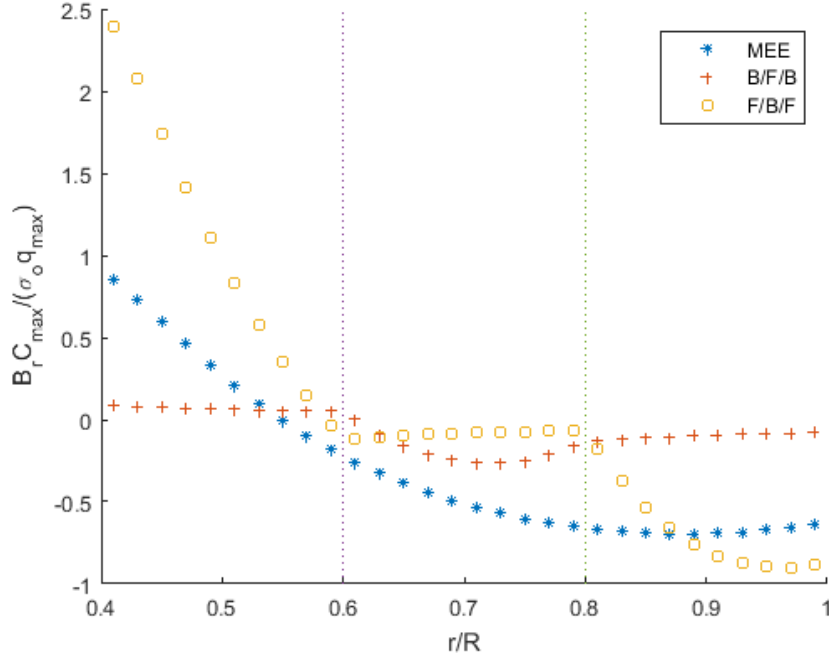
(c) Variation of magnetic potential component in layered hollow sphere composed of MEE materials subjected to axisymmetric external pressure q



(d) Variation of radial stress component in layered hollow sphere composed of MEE materials subjected to axisymmetric external pressure q



(e) Variation of radial electric displacement in layered hollow sphere composed of MEE materials subjected to axisymmetric external pressure q



(f) Variation of radial magnetic displacement in layered hollow sphere composed of MEE materials subjected to axisymmetric external pressure q

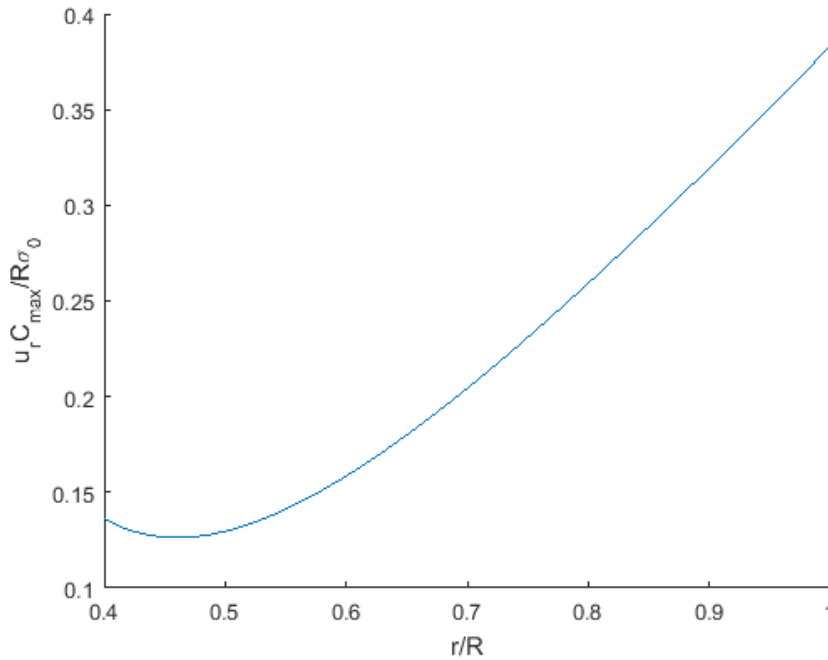
FIGURE 4.8. Plot demonstrating the variation of (A) dimensionless radial displacement $u_r C_{44}/(qr_2)$, (B) dimensionless electric potential $\phi e_{max}/\sigma_0$, and (C) dimensionless magnetic potential component $\psi q_{max}/\sigma_0$ (D) dimensionless radial stress σ_{rr}/σ_0 , (E) dimensionless radial electric displacement $D_r C_{max}/\sigma_0 e_{max}$, and (F) dimensionless radial magnetic displacement $B_r C_{max}/\sigma_0 q_{max}$ along the radial direction (r/R) in hollow sphere composed of magneto-electro-elastic (MEE) materials applied with an axisymmetric external pressure of q on its outer surface r_b .

4.6. HOLLOW MEE SPHERE UNDER THERMAL LOAD

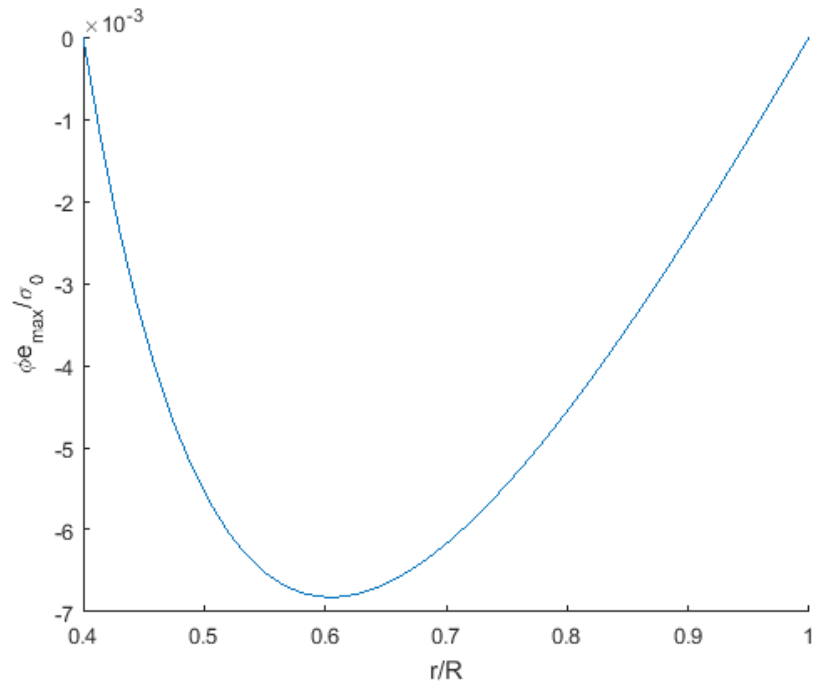
In this section, a homogeneous hollow MEE sphere is subjected to steady state thermal loads. A uniform temperature distribution is applied to the outer and inner surfaces of the hollow sphere of the previous examples. This is imposed as

$$T(0.4R, \zeta, \theta) = 0 \quad T(R, \zeta, \theta) = 1.0 \quad (4.6.1)$$

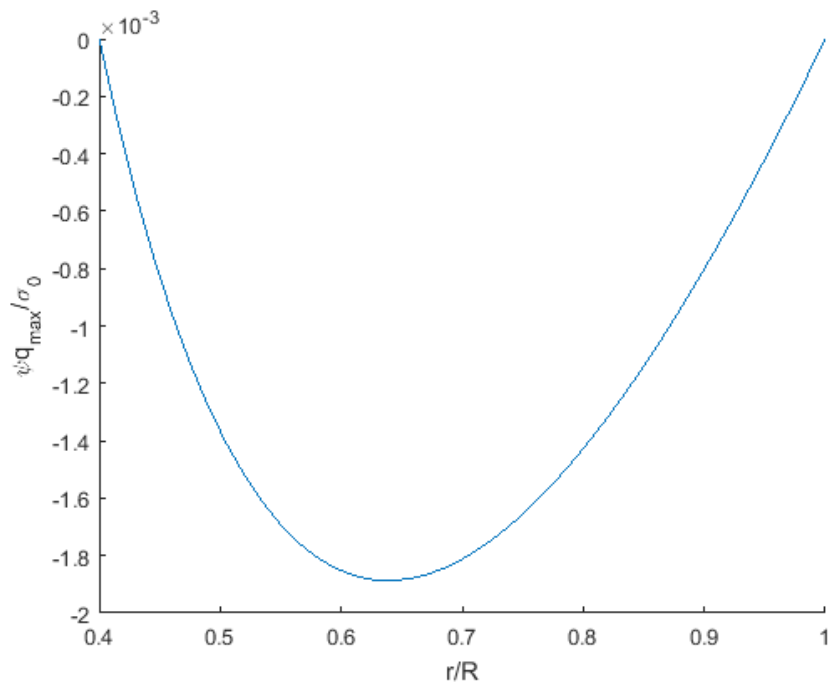
As in the case of a uniform pressure, a single term in (ζ, θ) can be used for the four non-zero field variables (u_r, ϕ, Ψ, T) that are all equal to unity. Hence the radial variation is captured by the discrete layer approximations. The pyroelectric and the pyromagnetic terms are equal to zero, since only the elastic and the thermal terms are coupled. For this problem, a homogeneous MEE layer composed of BaTiO_3 and CoFe_2O_4 with 20 percent volume fraction V_f , whose material properties are listed in Table 4.2. The dimensionless results are presented in Figure 4.9a- 4.9d. From Figure 4.9a, we observe that there is a very significant magnitude of radial displacement increase with the increase in the temperature distribution along through the thickness of the hollow sphere. The radial displacement is only governed by steady state thermal loading directly and this influences the electric and magnetic potentials indirectly. This behavior can be concluded from the Figure 4.9b and 4.9c. But these indirect effects are negligible.



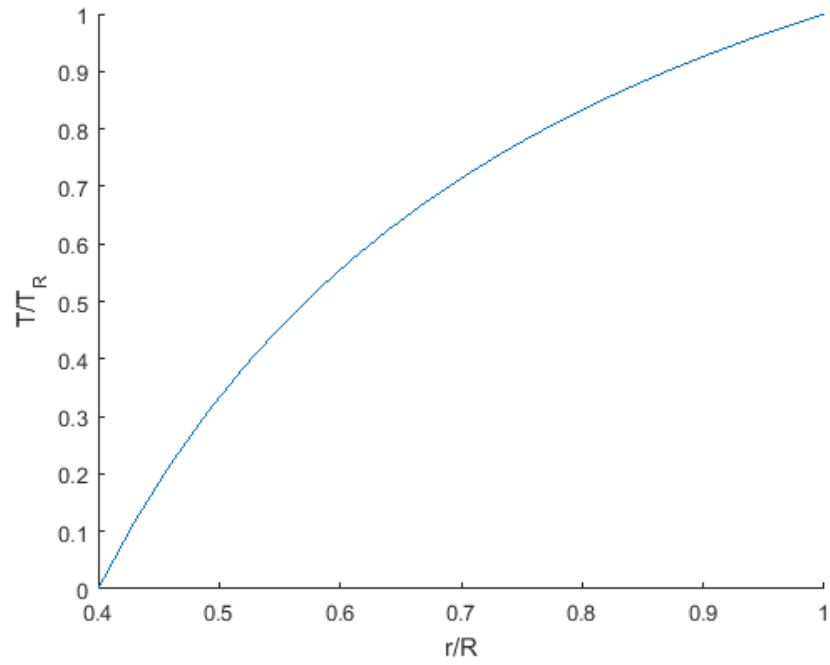
(a) Variation of radial displacement in purely elastic hollow sphere subjected to uniform pressure q



(b) Variation of radial displacement in purely elastic hollow sphere subjected to uniform pressure q



(c) Variation of temperature in purely elastic hollow sphere subjected to uniform pressure q



(d) Variation of temperature in purely elastic hollow sphere subjected to uniform pressure q

FIGURE 4.9. Plot demonstrating the variation of (A) dimensionless radial displacement $u_r C_{44}/(qr_2)$ and (B) dimensionless temperature change (T/T_R) along the radial direction (r/R) in a purely elastic hollow sphere applied with an uniform temperature distribution along its radial direction.

TABLE 4.2. The material properties used in this study for the piezoelectric (BaTiO₃), magnetostrictive (CoFe₂O₄), and MEE (50/50 mix) materials. The units of C_{ij} are 10⁹N/m², e_{ij} are C/m², q_{ij} are N/Am, ϵ_{ij} are 10⁻⁹ C²/(Nm²), μ_{ij} are 10⁻⁶ Ns²/C², α_{ij} are 10⁻¹² Ns/VC β_{ij} are 10⁶ N/m²K, k_{ij}^T are N/sK

Property	BaTiO ₃	CoFe ₂ O ₄	MEE($V_f=0.5$)	MEE($V_f=0.2$)
C_{11}	162.0	269.5	207.0	241.3
C_{22}	166.0	286.0	213.0	254.0
C_{12}	78.0	170.5	113.0	144.5
C_{13}	78.0	170.5	113.0	144.5
C_{23}	77.0	173.0	113.0	144.5
C_{33}	166.0	286.0	213.0	144.5
C_{44}	44.5	56.5	50.0	50.0
C_{55}	43.0	45.3	49.9	45.0
C_{66}	43.0	45.3	49.9	45.0
α_{11}	0.0	0.0	2750.0	2162.0
α_{33}	0.0	0.0	-5.23	2.8
e_{11}	18.6	0.0	8.86	3.412
e_{12}	-4.4	0.0	-2.71	-1.212
e_{13}	-4.4	0.0	-2.71	-1.212
e_{35}	11.6	0.0	0.15	-
e_{26}	11.6	0.0	0.15	-
ϵ_{11}	12.6	0.093	6.37	2.622
ϵ_{22}	11.2	0.08	0.24	0.33
ϵ_{33}	11.2	0.08	0.24	0.33
q_{11}	0.0	699.7	292.0	516.2
q_{12}	0.0	580.3	222.0	417.2
q_{13}	0.0	580.3	222.0	417.2
q_{35}	0.0	550.0	185.0	-
q_{26}	0.0	550.0	185.0	-
μ_{11}	10.0	157.0	83.9	130.5
μ_{33}	5.0	590.0	201.0	-
β_{11}	-	-	-	5.60
k_{11}^T	-	-	-	1.2

CHAPTER 5

SUMMARY AND CONCLUSIONS

In this study, approximate solutions to the weak form of the governing equations of equilibrium, electric flux, magnetic flux, heat flux are obtained for a hollow sphere containing n layers, that is made up of anisotropic magneto-electro-elastic material in a steady-state thermal field under static condition. On application of a load, the sphere undergoes deformation and, there is a coupling of these fields and the conversion of energy from one form to another is represented by consideration of the independent ritz-based approximations for each of these fields. By setting these variables unknowns layer-wise through the thickness in an approximate discrete-layer model, the unknowns are found out. As numerical illustrations, results have been presented for one-dimensional and two-dimensional analysis for three layered hollow sphere composed of piezoelectric barium titanate BaTiO_3 and magnetostrictive cobalt ferrite CoFe_2O_4 and the single layer MEE material under external uniform pressure and axisymmetric loading conditions. The study of the effects of physical laminate schemes of B/F/B, F/B/F and the MEE spheres. The influence of layer sequence, number of layers, multiphase couplings due to elastic, electric, magnetic and thermal fields are illustrated. The results obtained from the present model will serve as valuable reference to the analysis of multilayered magneto-electro-thermoelastic sphere based on various analytical methods.

5.1. CONCLUSIONS

The following conclusions have been drawn from this research:

- The radial displacement and temperature change obtained from the approximate model proved to match explicitly with the exact solution for purely elastic sphere subjected to thermal loads.
- The radial displacement, electrostatic and magnetic potential have been effected by change in slope due to dissimilar layers of B/F/B and F/B/F through the thickness of hollow sphere. But, the coupled MEE sphere did not suffer such an effect under the uniform external pressure.
- It was observed that the homogeneous coupled MEE hollow sphere under the uniform external pressure has the most significant value of electric displacement and magnetic induction when compared to the laminate schemes used in this study.
- The laminate sequence B/F/B showed the most significant electric displacement and laminate sequence F/B/F exhibited highest magnitude of magnetic induction, which was true for both the cases on the innermost layer when subjected to axisymmetric loading.
- The radial displacement is only governed by steady state thermal loading directly by thermoelastic coupling and this influences the electric and magnetic potentials indirectly. But the indirect effects are negligible.

5.2. FUTURE WORK

- A fully coupled thermo-magneto-electro elastic hollow sphere could be studied to investigate the other product properties such as pyroelectric and pyromagnetic coefficients.
- Moisture loads could be applied to the MEE hollow sphere to investigate its effects,

in addition to the thermal loads.

- A behaviour of MEE sphere under transient thermal load could be studied.
- A free vibration analysis of the MEE sphere could be considered as MEE hollow spheres are used in spherical acoustics

BIBLIOGRAPHY

- [1] Q.-H. Qin and Q.-S. Yang, *Macro-micro Theory on Multi-field Coupling Behavior of Heterogeneous Materials*. Berlin: Springer, 2008.
- [2] G. Haertling, “Ferroelectric ceramics - history and technology,” *Journal of the American Ceramic Society*, vol. 82(4), pp. 797–818, 1999.
- [3] H. Mahboubeh, Z. Fatemeh, and et al, “Synthesis of cobalt ferrite (cofe₂o₄) nanoparticles using combustion, coprecipitation, and precipitation methods: A comparison study of size, structural, and magnetic properties,” *Journal of Magnetism and Magnetic Materials*, vol. 371, pp. 43–48, 2014.
- [4] A. Akbarzadeh and D. Pasini, “Multiphysics of multilayered and functionally graded cylinders under prescribed hygrothermomagnetolectromechanical loading,” *ASME Journal of Applied Mechanics*, vol. 81:041018, 2014.
- [5] P. Penfield and A. Hermann, *Electrodynamics of moving media, Research Monograph*. No. 40, The MIT Press, Cambridge MA, 1967.
- [6] N. Pagano and J. Reddy, *Mechanics of composite materials: Selected works of Nicholas J. Pagano*, vol. 34. Kluwer Academic Publishers, Dordrecht, 1994.
- [7] J. Reddy, “A general nonlinear third-order theory of plates with moderate thickness,” *International Journal of Non-Linear Mechanics*, vol. 25(6), p. 677686, 1990.
- [8] P. Curie, “Physique, 3i’eme s’eries 111,” *journal*, 1894.
- [9] P. Debye, “title,” *Z.Phys*, vol. 36, p. 300, 1926.
- [10] L. Landau and E. Lifshitz, “Electrodynamics of continuous media,” *Pergamon Press*, 1960.
- [11] D. Astrov, “Soviet physics,” *Journal of Experimental and Theoretical Physics*, vol. 11, p. 708, 1960.

- [12] N. Hill, “Why are there so few magnetic ferroelectrics,” *The Journal of Physical Chemistry*, vol. 104 (29), pp. 6694–6709, 2000.
- [13] D. Khomskii, “Multiferroics: different ways to combine magnetism and ferroelectricity,” *Journal of Magnetism and Magnetic Materials*, vol. 306, pp. 1–8, 2006.
- [14] A. C. Vaz, J. Hoffman, and et al, “Magnetolectric coupling effects in multiferroic complex oxide composite structures,” *Advanced Materials*, vol. 22, pp. 2900–2918, 2010.
- [15] Manjusha and K. Yadav, “Structural, dielectric and magnetic properties of 0.3cofe2o4-0.7batio3-pvdf composite film,” *Smart Materials Letters*, vol. 5(11), pp. 652–657, 2014.
- [16] J. V. Suchtelen, “Product properties: a new application of composite materials,” *Philips Research Reports*, vol. 27, pp. 28–37, 1972.
- [17] K. Challagulla and A. Georgiades, “Micromechanical analysis of magneto-electrothermo-elastic composite materials with application to multilayered structures,”
- [18] J. V. den Boomgaard, D. Terrell, and et al, “An insitu grown eutectic magnetolectric composite material: part 1, composition and unidirectional solidification,” *Journal of Material Sciences*, vol. 9, pp. 1705–1709, 1974.
- [19] P. Lee, “A variational principle for the equations of piezoelectromagnetism in elastic dielectric crystals,” *Journal of Applied Sciences*, vol. 6, pp. 7470–7473, 1991.
- [20] J. He, “Variational theory for linear magneto-electroelasticity,” *International Journal of Nonlinear Sciences and Numerical Simulations*, vol. 2, pp. 309–316, 2001.
- [21] G. Qing, J. Qir, and et al, “Modified h-r mixed variational principle for magneto-electroelastic bodies and state-vector equation,” *Applied Mathematics and Mechanics*, vol. 2, pp. 309–316, 2001.

- [22] A. Soh and J. Lui, “On the constitutive equations of magneto-electroelastic solids,” *Journal of Intelligent Material Systems and Structures*, vol. 16, pp. 597–602, 2005.
- [23] J. Chen, E. Pan, and P. Heyliger, “Static deformation of a spherically anisotropic and multilayered magneto-electro-elastic hollow sphere,” *International Journal of Solids and Structures*, vol. 60, pp. 66–74, 2015.
- [24] E. Pan, “Exact solution for simply supported and multilayered magneto-electro-elastic plates,” *Journal of Applied Mechanics*, vol. 68, pp. 608–613, 2001.
- [25] E. Pan and P. Heyliger, “Free vibrations of simply supported and multilayered magneto-electroelastic plates,” *Journal of Sound & Vibration*, vol. 252, pp. 429–442, 2002.
- [26] X. Jiang and E. Pan, “Exact solution for 2d inclusion problem in anisotropic magneto-electroelastic full-, half- and bi-material-planes,” *International Journal of Solids and Structures*, vol. 41, pp. 4361–4382, 2004.
- [27] P. Heyliger and E. Pan, “Static fields in magneto-electroelastic laminates,” *The American Institute of Aeronautical and Astronautics Journal*, vol. 42, pp. 1435–1443, 2004.
- [28] P. Heyliger, E. Ramirez, and E. Pan, “Two-dimensional static fields in magneto-electroelastic laminates,” *Journal of International Material Systems and Structures*, vol. 15, pp. 689–709, 2004.
- [29] H. Yang, S. Saigal, and et al, “A survey of recent shell finite elements,” *International Journal for Numerical Methods in Engineering*, vol. 47(1-3), pp. 101–127, 2000.
- [30] J. Reddy, *Mechanics of Laminated Composite Plates and Shells: Theory and Analysis*. CRC Press, Boca Raton, Florida, 2nd ed., 2004.
- [31] W. Koiter, “A consistent first approximation in the general theory of thin elastic shells,” in *In Proceedings of the Symposium on Theory of Thin Elastic Shells (IUTAM), Delft*, pp. 12–33, August 24–28 1960.

- [32] A. Carrera, “A study of transverse normal stress effect on vibration of multilayered plates and shells,” *Journal of Sound and Vibration*, vol. 225(5), p. 803829, 1999.
- [33] S. Srinivas, C. Rao, and et al, “Flexural vibration of rectangular plates,” *Journal of Applied Mechanics*, vol. 23, p. 430436, 1970.
- [34] K. Bhaskar and T. Varadan, “Benchmark elasticity solution for locally loaded laminated orthotropic cylindrical shells,” *AIAA Journal*, vol. 34, 1994.
- [35] J. Reddy and C. Lui, “A higher-order shear deformation theory of laminated elastic shells,” *International Journal of Engineering Science*, vol. 23(3), pp. 319–330, 1985.
- [36] J. Garcao, C. Soares, and et al, “Analysis of laminated adaptive plate structures using layerwise finite element models,” *Computers and Structures*, vol. 82(23-26), p. 19391959, 2004.
- [37] M. Rao, Y. Desai, and et al, “Free vibrations of laminated beams using mixed theory,” *Computers and Structures*, vol. 63(3-4), p. 361373, 2004.
- [38] M. Rao and Y. Desai, “Analytical solutions for vibrations of laminated and sandwich plates using mixed theory,” *Composite Structures*, vol. 52(2), p. 149160, 2001.
- [39] R. Mindlin, “Equations of high frequency vibrations of thermopiezoelectric crystals plates,” *International Journal of Solid Structures*, vol. 10, pp. 625–637, 1974.
- [40] W. Nowacki, “Some general theorems of thermopiezoelectricity,” *Journal of Thermal Stresses*, vol. 1, pp. 171–182, 1978.
- [41] G. Altay and M. Dokmeci, “Fundamental variational equations of discontinuous thermopiezoelectric fields,” *International Journal of Engineering Sciences*, vol. 34, pp. 769–782, 1996.

- [42] G. Harshe, J. Dougherty, and et al, “Theoretical modelling of multilayered magneto-electric composites,” *International Journal of Applied Electromagnetics in materials*, vol. 4, pp. 145–159, 1993a.
- [43] C. Nan, “Magnetolectric effects in composites of piezoelectric and piezomagnetic phases,” *Physical Review B*, vol. 50, no. 22, pp. 6082–6088, 1994.
- [44] Y. Benveniste, “Universal relations in piezoelectric composites in eigenstress and polarization fields 11 multiphase media: Effective behavior,” *Journal of Applied Mechanics*, vol. 60, pp. 265–269, 1993a.
- [45] W. Chen, K. Lee, and et al, “General solution for transversely isotropic magneto-electro-thermo-elasticity and the potential theory method,” *International Journal of Engineering Sciences*, vol. 42, pp. 1361–1379, 2004.
- [46] W. Smittakorn and P. Heyliger, “A discrete-layer model of laminated hygrothermopiezoelectric plates,” *Mechanics of Composite Materials and Structures*, vol. 7, pp. 1–32, 2000.
- [47] Y. Ootao and M. Ishihara, “Exact solution of transient thermal stress problem of a multilayered magneto-electro-thermoelastic hollow sphere,” *Applied Mathematical Modelling*, vol. 36, pp. 1431–1443, 2012.
- [48] A. Bower, *Applied Mechanics of Solids*, ch. Solutions to simple boundary and initial value problems. publisher, 2008.
- [49] W. Chen, H. Ding, and et al, “Three-dimensional static analysis of multi-layered piezoelectric hollow spheres via the state space method,” *International Journal of Solids and Structures*, vol. 38, pp. 4921–4936, 2001.

- [50] H. Kuo and E. Pan, “Effective magnetoelectric effect in multicoated circular fibrous multiferroic composites,” *Journal of Applied Physics*, vol. 109: 104901, 2011.
- [51] M.L. Dunn and M. Taya, “An Analysis of Composite materials containing Ellipsoidal Piezoelectric Inhomogeneties,” *Proceedings: Mathematical and Physical Sciences*, vol. 443, 1993.

APPENDIX

The elements of the coefficient matrices for the discrete-layer model are simplest to express prior to the integration in radial direction. These include,

$$\begin{aligned}
K_{ij}^{11} &= \int_V \left[C_{11} \frac{\partial N_i^u}{\partial r} \frac{\partial N_j^u}{\partial r} + C_{12} \frac{N_i^u}{r} \frac{\partial N_j^u}{\partial r} + C_{13} \frac{N_i^u}{r} \frac{\partial N_j^u}{\partial r} \right. \\
&\quad C_{12} \frac{\partial N_i^u}{\partial r} \frac{N_j^u}{r} + \frac{C_{22}}{r^2} N_i^u N_j^u + \frac{C_{23}}{r^2} N_i^u N_j^u \\
&\quad \frac{C_{13}}{r} \frac{\partial N_i^u}{\partial r} N_j^u + \frac{C_{23}}{r^2} N_i^u N_j^u + \frac{C_{33}}{r^2} N_i^u N_j^u \\
&\quad \left. \frac{C_{55}}{r^2 \sin^2 \zeta} \frac{\partial N_i^u}{\partial \theta} \frac{\partial N_j^u}{\partial \theta} + \frac{C_{66}}{r^2} \frac{\partial N_i^u}{\partial \zeta} \frac{\partial N_j^u}{\partial \zeta} \right] r^2 \sin \zeta dr d\theta d\zeta \\
K_{ij}^{12} &= \int_V \left[\frac{C_{12}}{r} \frac{\partial N_i^u}{\partial r} \frac{\partial N_j^v}{\partial \zeta} + \frac{C_{22}}{r^2} N_i^u \frac{\partial N_j^v}{\partial \zeta} + \frac{C_{23}}{r^2} N_i^u \frac{\partial N_j^v}{\partial \zeta} \right. \\
&\quad \frac{C_{13} \cot \zeta}{r} \frac{\partial N_i^u}{\partial r} N_j^v + \frac{C_{23} \cot \zeta}{r^2} N_i^u N_j^v + \\
&\quad \frac{C_{33} \cot \zeta}{r^2} N_i^u N_j^v + \\
&\quad \left. \frac{C_{66}}{r} \frac{\partial N_i^u}{\partial \zeta} \left(\frac{\partial N_j^v}{\partial r} - \frac{N_j^v}{r} \right) \right] r^2 \sin \zeta dr d\theta d\zeta \\
K_{ij}^{13} &= \int_V \left[\frac{C_{13}}{r \sin \zeta} \frac{\partial N_i^u}{\partial r} \frac{\partial N_j^w}{\partial \theta} + \frac{C_{23}}{r^2 \sin \zeta} N_i^u \frac{\partial N_j^w}{\partial \theta} + \frac{C_{33}}{r^2 \sin \zeta} N_i^u \frac{\partial N_j^w}{\partial \theta} \right. \\
&\quad \left. \frac{C_{55}}{r \sin \zeta} \frac{\partial N_i^u}{\partial \theta} \left(\frac{\partial N_j^w}{\partial r} - \frac{N_j^w}{r} \right) \right] r^2 \sin \zeta dr d\theta d\zeta \\
K_{ij}^{14} &= \int_V \left[e_{11} \frac{\partial N_i^u}{\partial r} \frac{\partial N_j^\phi}{\partial r} + \frac{e_{12}}{r} N_i^u \frac{\partial N_j^\phi}{\partial r} + \frac{e_{13}}{r} N_i^u \frac{\partial N_j^\phi}{\partial r} + \frac{e_{26}}{r^2} \frac{\partial N_i^u}{\partial \zeta} \frac{\partial N_j^\phi}{\partial \zeta} + \right. \\
&\quad \left. \frac{e_{35}}{r^2 \sin^2 \zeta} \frac{\partial N_i^u}{\partial \theta} \frac{\partial N_j^\phi}{\partial \theta} \right] r^2 \sin \zeta dr d\theta d\zeta
\end{aligned}$$

$$\begin{aligned}
K_{ij}^{15} &= \int_V \left[q_{11} \frac{\partial N_i^u}{\partial r} \frac{\partial N_j^\Psi}{\partial r} + \frac{q_{12}}{r} N_i^u \frac{\partial N_j^\Psi}{\partial r} + \frac{q_{13}}{r} N_i^u \frac{\partial N_j^\Psi}{\partial r} + \frac{q_{26}}{r^2} \frac{\partial N_i^u}{\partial \zeta} \frac{\partial N_j^\Psi}{\partial \zeta} + \right. \\
&\quad \left. \frac{q_{35}}{r^2 \sin^2 \zeta} \frac{\partial N_i^u}{\partial \theta} \frac{\partial N_j^\Psi}{\partial \theta} \right] r^2 \sin \zeta dr d\theta d\zeta \\
K_{ij}^{16} &= \int_V -\beta_{11} \frac{\partial N_i^u}{\partial r} N_j^T r^2 \sin \zeta dr d\theta d\zeta \\
K_{ij}^{17} &= \int_V -\xi_{11} \frac{\partial N_i^u}{\partial r} N_j^M r^2 \sin \zeta dr d\theta d\zeta \\
K_{ij}^{22} &= \int_V \left[\frac{C_{22}}{r^2} \frac{\partial N_i^v}{\partial \zeta} \frac{\partial N_j^v}{\partial \zeta} + \frac{C_{23} \cot \zeta}{r^2} N_i^v \frac{\partial N_j^v}{\partial \zeta} + \frac{C_{32} \cot \zeta}{r^2} \frac{\partial N_i^v}{\partial \zeta} N_j^v \right. \\
&\quad \left. \frac{C_{33} \cot^2 \zeta}{r^2} N_i^v N_j^v + \frac{C_{44}}{r^2 \sin^2 \zeta} \frac{\partial N_i^v}{\partial \theta} \frac{\partial N_j^v}{\partial \theta} + \right. \\
&\quad \left. C_{66} \left(\frac{\partial N_i^v}{\partial r} - \frac{N_i^v}{r} \right) \left(\frac{\partial N_j^v}{\partial r} - \frac{N_j^v}{r} \right) \right] r^2 \sin \zeta dr d\theta d\zeta \\
K_{ij}^{23} &= \int_V \left[\frac{C_{23}}{r^2 \sin \zeta} \frac{\partial N_i^v}{\partial \zeta} \frac{\partial N_j^w}{\partial \theta} + \frac{C_{33}}{r^2 \sin \zeta} \cot \zeta N_i^v \frac{\partial N_j^w}{\partial \theta} + \right. \\
&\quad \left. \frac{C_{44}}{r^2 \sin \zeta} \frac{\partial N_i^v}{\partial \theta} \left(\frac{\partial N_j^w}{\partial \zeta} - \cot \zeta N_j^w \right) \right] r^2 \sin \zeta dr d\theta d\zeta \\
K_{ij}^{24} &= \int_V \left[\frac{e_{12}}{r} \frac{\partial N_i^v}{\partial \zeta} \frac{\partial N_j^\phi}{\partial r} + \frac{e_{13} \cot \zeta}{r} N_i^v \frac{\partial N_j^\phi}{\partial r} + \frac{e_{26}}{r} \left(\frac{\partial N_i^v}{\partial r} - \frac{N_i^v}{r} \right) \frac{\partial N_j^\phi}{\partial \zeta} \right] r^2 \sin \zeta dr d\theta d\zeta \\
K_{ij}^{33} &= \int_V \left[\frac{C_{33}}{r^2 \sin^2 \zeta} \frac{\partial N_i^w}{\partial \theta} \frac{\partial N_j^w}{\partial \theta} + \frac{C_{44}}{r^2} \left(\frac{\partial N_i^w}{\partial \zeta} - \cot \zeta N_i^w \right) \left(\frac{\partial N_j^w}{\partial \zeta} - \cot \zeta N_j^w \right) + \right. \\
&\quad \left. C_{55} \left(\frac{\partial N_i^w}{\partial r} - \frac{N_i^w}{r} \right) \left(\frac{\partial N_j^w}{\partial r} - \frac{N_j^w}{r} \right) \right] r^2 \sin \zeta dr d\theta d\zeta \\
K_{ij}^{34} &= \int_V \left[\frac{e_{13}}{r \sin \zeta} \frac{\partial N_i^w}{\partial \theta} \frac{\partial N_j^\phi}{\partial r} + \frac{e_{35}}{r \sin \zeta} \left(\frac{\partial N_i^w}{\partial r} - \frac{N_i^w}{r} \right) \frac{\partial N_j^\phi}{\partial \theta} \right] r^2 \sin \zeta dr d\theta d\zeta \\
K_{ij}^{35} &= \int_V \left[\frac{q_{13}}{r \sin \zeta} \frac{\partial N_i^w}{\partial \theta} \frac{\partial N_j^\Psi}{\partial r} + \frac{q_{35}}{r \sin \zeta} \left(\frac{\partial N_i^w}{\partial r} - \frac{N_i^w}{r} \right) \frac{\partial N_j^\Psi}{\partial \theta} \right] r^2 \sin \zeta dr d\theta d\zeta \\
K_{ij}^{44} &= \int_V \left[-\epsilon_{11} \frac{\partial N_i^\phi}{\partial r} \frac{\partial N_j^\phi}{\partial r} - \frac{\epsilon_{22}}{r^2} \frac{\partial N_i^\phi}{\partial \zeta} \frac{\partial N_j^\phi}{\partial \zeta} - \frac{\epsilon_{33}}{r^2 \sin^2 \zeta} \frac{\partial N_i^\phi}{\partial \theta} \frac{\partial N_j^\phi}{\partial \theta} \right] r^2 \sin \zeta dr d\theta d\zeta
\end{aligned}$$

$$K_{ij}^{45} = \int_V \left[-\alpha_{11} \frac{\partial N_i^\phi}{\partial r} \frac{\partial N_j^\Psi}{\partial r} - \frac{\alpha_{22}}{r^2} \frac{\partial N_i^\phi}{\partial \zeta} \frac{\partial N_j^\Psi}{\partial \zeta} - \frac{\epsilon_{33}}{r^2 \sin^2 \zeta} \frac{\partial N_i^\phi}{\partial \theta} \frac{\partial N_j^\Psi}{\partial \theta} \right] r^2 \sin \zeta dr d\theta d\zeta \quad (0.1)$$

$$K_{ij}^{55} = \int_V \left[-\mu_{11} \frac{\partial N_i^\Psi}{\partial r} \frac{\partial N_j^\Psi}{\partial r} - \frac{\mu_{22}}{r^2} \frac{\partial N_i^\Psi}{\partial \zeta} \frac{\partial N_j^\Psi}{\partial \zeta} - \frac{\mu_{33}}{r^2 \sin^2 \zeta} \frac{\partial N_i^\Psi}{\partial \theta} \frac{\partial N_j^\Psi}{\partial \theta} \right] r^2 \sin \zeta dr d\theta d\zeta$$

The element matrices for Elastic-Temperature Problem

$$K_{ij}^{11} = \int_V \left[C_{11} \frac{\partial N_i^u}{\partial r} \frac{\partial N_j^u}{\partial r} + C_{12} \frac{N_i^u}{r} \frac{\partial N_j^u}{\partial r} + C_{13} \frac{N_i^u}{r} \frac{\partial N_j^u}{\partial r} \right. \\ \left. C_{12} \frac{\partial N_i^u}{\partial r} \frac{N_j^u}{r} + \frac{C_{22}}{r^2} N_i^u N_j^u + \frac{C_{23}}{r^2} N_i^u N_j^u \right. \\ \left. \frac{C_{13}}{r} \frac{\partial N_i^u}{\partial r} N_j^u + \frac{C_{23}}{r^2} N_i^u N_j^u + \frac{C_{33}}{r^2} N_i^u N_j^u \right] r^2 dr$$

$$K_{ij}^{12} = \int_V \left[-\beta_{11} N_j^T \frac{\partial N_i^u}{\partial r} - \beta_{22} N_j^T \frac{N_i^u}{r} - \beta_{33} N_j^T \frac{N_i^u}{r} \right] r^2 dr$$

$$K_{ij}^{21} = 0$$

$$K_{ij}^{22} = \int_V \left[-K_1^T \left(\frac{\partial N_i^T}{\partial r} \frac{\partial N_j^T}{\partial r} + 2 \frac{\partial N_i^T}{\partial r} \frac{N_j^T}{r} + 2 \frac{\partial N_j^T}{\partial r} \frac{N_i^T}{r} + 4 \frac{N_i^T}{r} \frac{N_j^T}{r} \right) \right] r^2 dr$$